Complexation Behavior of Polyampholytes and Charged Objects

Roland R. Netz*,†,‡ and Jean-François Joanny†

Institut Charles Sadron, 6 rue Boussingault, 67083 Strasbourg, France
Max-Planck-Institut für Kolloid- und Grenzflächenforschung, Kantstrasse 55, 14513 Teltow, Germany

Received January 28, 1998; Revised Manuscript Received April 17, 1998

ABSTRACT: We study theoretically the interaction of a polyampholyte chain with charged planes, cylinders, and spheres. Due to the random character of the charge distribution along the chain, a polyampholyte possesses a spontaneous dipole moment, which can interact favorably with charged objects. Depending on the charge strength of the object and the polyampholyte length and fraction of charged monomers, this attractive interaction can be strong enough to induce adsorption. The addition of salt weakens the trend to adsorption, but proves necessary to adsorb polyampholytes of the same net charge as the charged object in the case of planes and cylinders. Long polyampholytes form globules, for which the number of uncompensated charges and thus the spontaneous dipole moment is reduced. Nevertheless, globules can adsorb on charged objects via two pathways: they either adsorb as a whole, (intact globule), or they are dissolved into a coil state prior to adsorption. Applications to the complexation behavior of polyampholytes with stiff, rodlike polyelectrolytes and with charged microspheres or charged spherical micelles are given.

I. Introduction

The combination of polymer physics with electrostatics provides a number of interesting theoretical questions and is associated with many experimental effects and applications. On the simplest level, one distinguishes the *polyelectrolyte* effect, obtained for polymers with charged monomers of the same sign, and the *polyampholyte* effect, for chains containing both positively and negatively charged monomers:

(i) Due to the strong repulsion between similarly charged monomers, polyelectrolytes (PE) tend to be highly swollen and stretched, and they dissolve even in solvents which are poor for the polymer backbone, e.g., hydrocarbons in water.[1] Added salt screens the electrostatic interactions and therefore reduces the stretching and leads to a reduction in the chain size.

(ii) For polyampholytes (PA), the attraction between oppositely charged monomers leads to a chain collapse, counteracted by a three-body repulsion.[2−4] The resulting PA globules show a drastically reduced solubility and usually form a precipitated phase. Added salt again weakens the polyampholyte effect and therefore leads to a characteristic globule swelling.

In this paper we systematically investigate the interaction of PA chains with charged objects. As objects, we choose the simplest geometries, namely planes, cylinders, and spheres. Experimentally, these different geometries can be realized in PA adsorption experiments at (i) charged surfaces (e.g., monolayers of charged surfactants or lipids at an air−water interface), (ii) charged linear macromolecules such as DNA, tubulin, or other stiff polyelectrolytes, and (iii) charged spherical particles, such as latex or silica beads, or charged surfactant micelles. In fact, a whole number of experiments have been performed on mixtures of gelatin (a biological PA) with ionic surfactants,[5−7] and have been interpreted in terms of a strong complexation between the PA and the charged, spherical micelles. The same conclusion has been reached in recent experiments on the complexation behavior of charged surfactants with synthetic polyampholytes.[8] In a different series of experiments, synthetic PA were shown to aggregate on charged latex particles.[9] The spectacular result of this last experiment was that PA can even adsorb if their overall charge has the same sign as that of the latex particle. This finding has been explained theoretically using a replica-calculation for the adsorption of PA on a charged wall for high salt concentration,[10] when the electrostatic interaction is very short-ranged. This calculation has been extended to weak screening,[11] but with the same main result: A PA chain strongly interacts with a flat charged surface and can adsorb even if the chain has a net charge of the same sign as the surface.

In this article we introduce a general Flory theory for the behavior of PA chains in external, nonhomogeneous electrostatic potentials. We apply our method to the electrostatic potentials created by charged walls, cylinders, and spheres. The counterions play an important role and show very distinctive behaviors for these three geometries: in the absence of salt, the charged wall binds all its counterions in a loose layer with a thickness given by the Gouy−Chapman length λ. In contrast, the electrostatic potential created by a single charged sphere is not strong enough to bind its counterions if the whole system is contained in an infinitely large box. The charged cylinder shows a somewhat intermediate behavior, in the sense that it can bind a fraction of its counterions in a diffuse layer above a certain line-charge density (as detailed in Appendix A). Below this specific line-charge density, which demarks the Manning condensation threshold, no counterions are bound to the cylinder. The different counterion distributions lead to different electrostatic potentials and therefore influence the PA adsorption behavior, which turns out to be different for the different geometries considered. For all three geometries, we find the adsorption of similarly charged PA to be possible, but for planes and cylinders this is obseved only in the presence of salt. For the

* To whom correspondence should be addressed at athe Max-Planck-Institut für Kolloid- und Grenzflächenforschung.
† Institut Charles Sadron.
‡ Max-Planck-Institut für Kolloid- and Grenzflächenforschung,

S0024-9297(98)00115-6 CCC: $15.00
Published on Web 07/01/1998

adsorption of PA globules we find two different pathways: they can either adsorb as a whole, intact globule, or be dissolved into a PA coil prior to adsorption.

The outline of our article is as follows: In section II we introduce our Flory model for the PA adsorption in an arbitrary external electrostatic potential and apply it to charged planar surfaces. For the adsorption of globules we first calculate the dipole moment of a PA globule, which is found to be much smaller than for a PA coil, as shown in Appendix B. Still, globule adsorption is possible. For the case of a PA with a net charge, we first calculate the scaling diagram without the influence of a charged surface, which shows PE behavior, PA globular behavior, and, for large salt concentration or small net charge fraction, a salty version of PA globules. In section III these results are applied to charged cylinders, which simply involves a rescaling of the parameters. In section IV, we consider the adsorption on charged spheres, which differs from the other two geometries because the surface of a sphere is finite and thus the repulsive interaction between adsorbed PA blobs must be taken into account. As a result, we find a maximal number of PA monomers which can adsorb on a sphere; the excess nonadsorbed PA portion coexists with the adsorbed chain portion. Finally, in the discussion we mention further applications of our results to recent experimental work.

II. Polyampholytes at Charged Planar Surfaces

In this section we introduce the Flory theory used in this article to describe the adsorption of a polyampholyte chain on a charged object, and apply it to the adsorption on a planar charged surface. This problem has been treated before with a somewhat simpler formalism.[11] As shown below, we obtain agreement with those results. This gives some justification to apply our Flory method to the other geometries, charged cylinders, and spheres, in sections III and IV.

We consider a polyampholyte coil with a fraction $f \equiv f_- + f_+$ of charged monomers, where f_+ and f_- denote the fractions of positive and negative charges on the chain, respectively. First, we are concerned with the case of a neutral PA chain, for which $\Delta f \equiv f_+ - f_- = 0$. In section II.D, we also discuss chains which have an average net charge $\Delta f \neq 0$. If the chain is not in the collapsed state, that is, if the chain is rather short or the charges are very dilute, the interactions between the charges are not important and the spontaneous charge fluctuations can be easily calculated: if one divides the coil of N monomers into two halves, there are on average $\tilde{Q} \sim (fN)^{1/2}$ divided charges.[11,12] A polyampholyte chain thus constitutes a permanent dipole. Qualitatively, this argument remains true if the chain is in a collapsed state; in this case, however, the strength of the permanent dipole is much reduced compared to this simple estimate. A model based on dipolar interactions (and ignoring higher order multipoles) presented in Appendix B suggests that $\tilde{Q}_g \sim (N/f)^{1/6}$ for PA globules. Upon interaction with a charged object, this spontaneous dipole orients itself such as to create an *attractive* interaction. Complete orientation is realized when the accompanying interaction strength is on the order of the thermal excitation energy k_BT. Throughout this paper, this also serves as our criterion for the adsorption of a PA coil or globule on a charged object. Since the thresholds for complete orientation and adsorption of a coil coincide, we always assume the adsorbed coil to be oriented favorably, i.e., with the oppositely charged half facing the charged object. Our model for the adsorption geometry is depicted in Figure 1. The stretched coil of polymerization index N is at an average distance z_0 from the surface of the charged object. The coil is divided into two halves, with mass and charge centers separated from each other by a distance z. The naive picture given in Figure 1 is certainly oversimplified. A more refined model would be to assume that the two half-chains have different sizes z_1 and z_2. We checked that this slightly more realistic model leads to the same conclusion as the simplest model. In the spherical geometry, it does eliminate some artifacts of the simple model but as these artifacts are of no significance for the final results, we stick to the simple model of Figure 1.

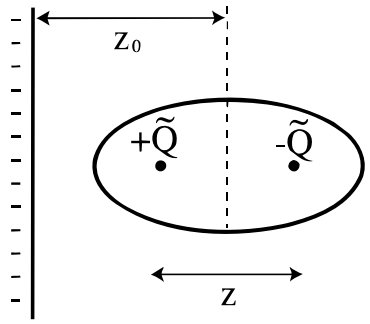

Figure 1. Schematic picture of the adsorption geometry. The polyampholyte coil is divided into two halves, which contain $\tilde{Q}$ separated charges each. The center of mass is a distance z_0 away from the negatively charged wall; the coil is oriented such as to maximize the attraction, pointing the positively charged half toward the wall. The separation between the two charge centers is z and can be larger than the equilibrium coil radius; i.e., the coil can be stretched.

The potential distribution for a charged plane in the presence of counterions at a distance x from the surface is[13]

$$\frac{eV_P(x)}{k_BT} = 2\ln(1 + x/\lambda) \tag{1}$$

where

$$\lambda \equiv \frac{2k_BT\epsilon}{e^2\sigma} \equiv \frac{1}{2\pi\sigma l_B} \tag{2}$$

is the so-called Gouy−Chapman length and σ denotes the surface charge density. The Bjerrum length $l_B \equiv e^2/4\pi\epsilon k_BT$ equals the length scale at which two unit charges interact with the thermal energy. The Gouy−Chapman length λ corresponds to the distance of a single ion from the charged wall at which its bare interaction with the wall is on the order of k_BT. The planar potential eq 1 follows from a solution of the Poisson−Boltzmann equation and describes the counterion distribution $n(x) \sim \exp(-eV_P(x)/k_BT)$ correctly on the mean-field level, neglecting correlations between counterion fluctuations. The deviation of eq 1 from the bare potential of a charged wall, $eV(x)/k_BT \sim 2x/\lambda$ is solely due to the presence of counterions. As can be checked by simple substitution, the Gouy−Chapman length corresponds to the scale over which half the counterions are bound to the surface. Although all counterions are bound to the wall, the outer ions are bound so loosely that the electric potential still diverges

logarithmically. The planar electrostatic energy W_P of the polyampholyte coil with a geometry depicted in Figure 1 is then

$$\frac{W_P}{k_B T} \approx \tilde{Q}(V_P(z_0 - z/2) - V_P(z_0 + z)) = -4\tilde{Q}\ \mathrm{arctanh}\left(\frac{z}{2\lambda + 2z_0}\right) \quad (3)$$

where $\tilde{Q}$ is the number of separated charges in the two PA halves. In eq 3, we assume the electrostatic potential to be unperturbed by the presence of the PA chain. This approximation is justified only for small local charge distributions, which is the case for the adsorbed PA phases found in this article.

The electric field stretches the coil by separating the two charges; this is associated to a free energy penalty due to the loss of entropy of the Gaussian coil. The total free energy of the polyampholyte in the field is (up to unimportant multiplicative factors)

$$\frac{F_P}{k_B T} \sim \frac{z^2}{a^2 N} - \sqrt{fN}\ \mathrm{arctanh}\left(\frac{z}{2\lambda + 2z_0}\right) \quad (4)$$

where we used the estimate $\tilde{Q} \sim (fN)^{1/2}$ which is valid if the PA is not in the globular state. This free energy is based on the assumption that the external electric field only acts on preexisting separated charges and does not change the chain statistics on small length scales, i.e., that the the field does not change the number of uncompensated charges $\tilde{Q}$. This is in fact true if the electric field is uniform: The large scales dominate the behavior.[11] If the field is nonuniform, this is no longer always true. The resulting behavior can still be described by the free energy expression eq 4 if one allows the chain to decorrelate into multiple blobs, thereby increasing the number of separated charges; this will be treated in section II.A. The free energy is smallest for minimal values of z_0; in the following we therefore do not consider a finite distance between the coil and the planar surface and set $z_0 = z$. The equilibrium state of the stretched coil is determined by a minimization with respect to z. For the limiting cases $z \gg \lambda$ and $z \ll \lambda$, the solutions are easily calculated. Using the dimensionless parameter for the Gouy−Chapman length

$$\tilde{\lambda} \equiv \lambda/a\sqrt{N} \quad (5)$$

the asymptotic solutions are

$$z \sim \begin{cases} a\sqrt{N}\ \tilde{Q}/\tilde{\lambda} & \text{for } z < \lambda \\ a\sqrt{N}\ (\tilde{Q}\tilde{\lambda})^{1/3} & \text{for } z > \lambda \end{cases} \quad (6)$$

By construction, these solutions are only meaningful if the chain is stretched, i.e. if $z > aN^{1/2}$. The solution for $z < \lambda$ is thus only valid for $\tilde{Q}/\tilde{\lambda} = af^{1/2}N/\lambda > 1$, and the solution for $z > \lambda$ is thus only valid for $\tilde{Q}\tilde{\lambda} = f^{1/2}\lambda/a > 1$. Outside these limits of validity, the PA coil is unperturbed and shows Gaussian statistics; i.e., $z \sim aN^{1/2}$. The crossover between the two solutions described in eq 6, at which the coil size equals the Gouy−Chapman length, occurs when $\tilde{Q}/\tilde{\lambda} \sim (\tilde{Q}\tilde{\lambda})^{1/3} \rightarrow \tilde{Q}^2/\tilde{\lambda}^4 \sim fN^3a^4\lambda^4 \sim 1$. The resulting chain behavior is the following: for $f < f_f \equiv a^2\lambda^{-2}$ the PA coil is not deformed and remains Gaussian. For $f > f_f$, on the other hand, the PA coil remains unstretched only for short chains but is stretched for longer chains. One observes that in fact a strongly charged surface is less able to perturb a PA coil; this has to do with the fact that the electric field for a strongly charged wall only extends over a short distance, namely the Gouy−Chapman length λ. In order to estimate whether the attractive electrostatic interaction is strong enough to bind the coil, we calculate the free energies for the two different solutions in eq 6. For the parameter range where a long PA chain is perturbed, i.e. for $f > f_f$, the result is

$$\frac{F_P}{k_B T} \sim \begin{cases} -fa^2N^2/\lambda^2 \sim -\tilde{Q}^2/\tilde{\lambda}^2 & \text{for } z \ll \lambda \\ (f\lambda^2a^2)^{1/3} - \sqrt{fN} \sim (\tilde{Q}\tilde{\lambda})^{2/3} - \tilde{Q} & \text{for } z \gg \lambda \end{cases} \quad (7)$$

Right at the crossover between the two solutions, for $z \approx \lambda$, the free energy is given by $F_P/k_BT \sim -\tilde{Q}$. At the boundary between the stretched and the unstretched solution, i.e., for $\tilde{Q}/\tilde{\lambda} \sim 1$, the adsorption free energy reaches the order of k_BT. The onset of stretching therefore demarks the adsorption boundary.

For $f < f_f$, the parameter range where the PA chain is always Gaussian, the adsorption energy can only be larger than unity when the coil is larger than the Gouy−Chapman length; it is then given by

$$\frac{F_P}{k_B T} \sim -\sqrt{fN} \sim -\tilde{Q} \quad (8)$$

When this adsorption energy reaches unity one enters the regime of diffuse adsorption, which is obtained for $\tilde{Q} > 1$ or $f > 1/N$.

A. Blob Formation. The N-dependence of the free energy for large coils suggests the formation of blobs: both for stretched and unstretched adsorbed coils, when $z > \lambda$, at large values of N, the leading term in the free energy, eqs 7 and 8, is proportional to $\sim N^{1/2}$. By breaking the coil up into g blobs with N/g monomers each, the free energy becomes linear in N, which is asymptotically always favorable. The size of the blobs can then be obtained by minimizing the free energy per monomer.

For the stretched adsorbed state, i.e. for $\tilde{Q}\tilde{\lambda} > 1$ or $f > f_f$, the blob size is determined by the coil size at the crossover between the two scaling regimes (N^2 behavior of the free energy, for $z < \lambda$, and square root behavior, for $z > \lambda$). This crossover takes place when the number of monomers is such that $\tilde{Q} \sim \tilde{\lambda}^2$, and the number of monomers per blob, N_b, is therefore $N_b \sim (\lambda^4/a^4f)^{1/3} \sim (\tilde{Q}\tilde{\lambda})^{4/3}/f$. The free energy gain of a polyampholyte chain of N_b monomers (one blob) is $F/k_BT \sim -(\tilde{Q}\tilde{\lambda})^{2/3}$. The adsorption free energy per blob thus can be much larger than k_BT, depending on the value of $\tilde{Q}\tilde{\lambda}$; this regime is therefore a *strong adsorption* (or fence) regime.

For the unstretched adsorbed state, i.e., for $\tilde{Q}\tilde{\lambda}$ or $f < f_f$, the blob size is determined by the condition that the adsorption free energy is larger than the thermal energy in order to overcome the entropy loss caused by decorrelating the coil into separate blobs. Using the adsorption free energy eq 8 for a Gaussian coil, we obtain as the blob-formation threshold $(fN)^{1/2} \approx 1$. The monomer blob size is therefore $N_w \sim 1/f$. The free energy gain per blob is of the order of k_BT, so that this is a *weak adsorption* regime.

The partitioning into g uncorrelated blobs costs a free energy of k_BT per blob. The free energies for g adsorbed

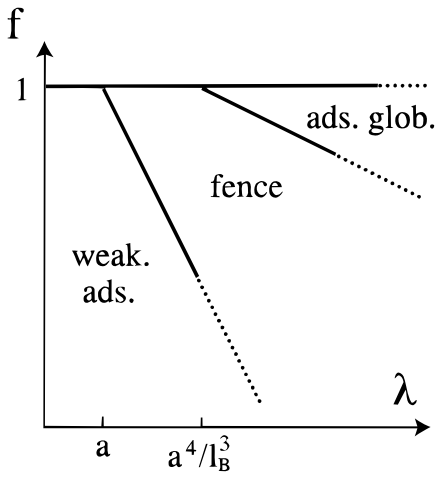

Figure 2. Adsorption phase diagram for an infinitely long neutral PA chain on a planar charged surface as a function of the charged-monomer fraction f and the Gouy−Chapman length $\lambda \sim 1/\sigma l_B$. For strongly charged surfaces or PA chains with few charged monomers, $f < f_f \equiv a^2/\lambda^2$, the PA is weakly adsorbed in a diffuse layer of thickness $R_z \sim a/\sqrt{f}$. For weakly charged surfaces, $f > f_{ag} \equiv a^2/\lambda^{1/2}l_B^{3/2}$, the PA adsorbs as a globule. In between, for $f_f < f < f_{ag}$, the PA strongly adsorbs as a fence with thickness $R_z \sim \lambda$. Double-logarithmic scales are used.

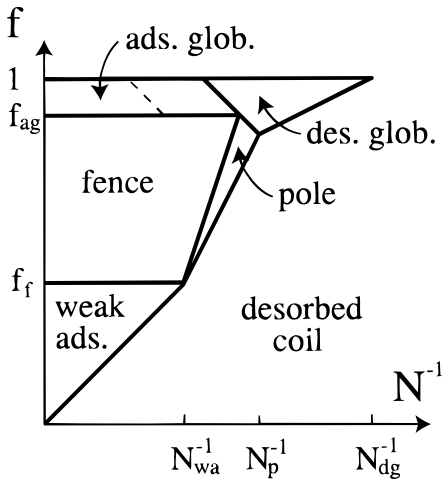

Figure 3. Adsorption phase diagram for a neutral PA chain at a weakly charged planar surface (for $\lambda > a^4/l_B^3$) as a function of the inverse chain length N^{-1} and the charged-monomer fraction, f. Double-logarithmic scales are used. We distinguish the pole regime, where the chain adsorbs as a stretched single coil, the fence regime with strong multiblob adsorption, and the regime of weak multiblob adsorption. Note that globules, which correspond to the equilibrium PA structure for $f > a/N^{1/2}l_B$, can adsorb as a whole, for $f > f_{ag}$, or be dissolved into an adsorbed multiblob structure, for $f < f_{ag}$. This phase diagram also applies to the adsorption on charged cylinders with a suitable redefinition of parameters explained in section III.

blobs are for the strong and weak adsorption regime, respectively, given by

$$\frac{F_p}{k_B T} \sim \begin{cases} \frac{N}{N_b}(1 - (\tilde{Q}\tilde{\lambda})^{2/3}) & \text{for } \tilde{Q} > \tilde{\lambda}^2 \\ -\frac{N}{N_w} & \text{for } \tilde{Q} > 1 \end{cases} \tag{9}$$

The boundary between these two blob regimes is given by $\tilde{Q}\tilde{\lambda} \sim 1$, where the free energies show a smooth crossover. In the strong adsorption regime, for $\tilde{Q}\tilde{\lambda} > 1$, the size of the adsorbed polymer layer is of the order of the Gouy−Chapman length, $R_z \sim \lambda$. In the weak adsorption regime, for $\tilde{Q}\tilde{\lambda} < 1$, the adsorbed layer has a thickness $R_z \sim aN_w^{1/2} \sim a/f^{1/2}$ and is thus on the order of the Gaussian real-space distance between charges.

The different adsorption regimes in the limit of an infinitely long PA chain, $N \to \infty$, are shown in Figure 2 as a function of the charged-monomer fraction f and the Gouy−Chapman length λ. We first note that an infinitely long chain is *always* adsorbed. The boundary between the weakly adsorbed and the fence regime is given by $f \sim f_f \equiv a^2\lambda^{-2}$ and hits the boundary $f = 1$ at $\lambda = a$. In the limit of a strongly charged surface, for $\lambda < a$, the chain is weakly adsorbed for all values of f with a diffuse thickness $R_z \sim a/f^{1/2}$ independent of the surface charge. We also show the transition between the fence and the adsorbed-globule regime, $f \sim f_{ag} \equiv a^2/\lambda^{1/2}l_B^{3/2}$, which is derived in section II.B. We always implicitly assume $l_B < a$, which is the realistic choice. For weakly charged surfaces, $\lambda > a^4/l_B^3$, we obtain three different adsorbed phases for different values of f. For this range of λ we show the resulting adsorption behavior in Figure 3 as a function of the charged monomer fraction f and the inverse chain length N^{-1}.

We distinguish the *single-coil adsorption or pole regime*, for $\tilde{\lambda}^2 < \tilde{Q}\tilde{\lambda} < \tilde{\lambda}^3$ (or $\lambda^2/a^2N^2 < f < \lambda^4/a^4N^3$), in which the polyampholyte adsorbs in a single, stretched coil of vertical size smaller than the Gouy−Chapman length, i.e., $R_z < \lambda$, the *strong adsorption or fence regime*, for $\tilde{\lambda}^3 < \tilde{Q}\tilde{\lambda}$ and $1 < \tilde{Q}\tilde{\lambda}$ (or $f > \lambda^4/a^4N^3$ and $f_f < f < f_{ag}$), where the polyampholyte adsorbs in multiple blobs with a vertical size comparable to the Gouy−Chapman length, and the *weak adsorption regime*, for $\tilde{\lambda} < \tilde{Q}\tilde{\lambda} < 1$ (or $1/N < f < f_f$), where the polyampholyte adsorbs in multiple blobs of size $a/f^{1/2}$ with an adsorption energy of roughly $1k_BT$ per blob. The constant $N_{wa} \equiv \lambda^2/a^2$ denotes the monomer threshold above which the weakly adsorbed region is observed. In the part of the phase diagram in which $f < N^{-1}$, the PA is never adsorbed. This is not surprising, since here the number of charged monomers per PA is smaller than unity. For large values of the charged monomer fraction f one observes regions of desorbed and adsorbed globular PA.

B. Adsorption of Polyampholyte Globules. So far we neglected interactions between charges within the polyampholyte coil. In the following we both give the conditions under which this simplification is accurate and the additional effects which occur when this simplification breaks down, i.e., for strongly interacting PA's. Unlike charges attract each other and can lead to a collapse of a polyampholyte.[2,3] The equilibrium density within such a polyampholyte globule of radius R_g is determined by a balance between the repulsive third virial term in a free energy expansion $\sim wN^3a^6/R_g^6$ and the attractive self-screening interaction between ions $\sim (fNl_B/R_g)^{3/2}$.[3] In the following, the third virial coefficient w is set to unity. For a polymerization index larger than the Debye number

$$N_D \equiv \left(\frac{a}{fl_B}\right)^2 \tag{10}$$

the polyampholyte is in the globular state. This condition can be reexpressed as $f > a/\sqrt{N}l_B$ and defines the boundary between the desorbed-coil and desorbed-globular regimes in Figure 3; it meets the boundary between the pole and desorbed-coil regimes at $N \sim N_p$

$\equiv \lambda^{4/3} l_B^{2/3}/a^2$ and the boundary $f = 1$ at $N \sim N_{dg} \equiv a^2/l_B^2$. The density in the globular state is independent of the chain length, and the globular chain radius is

$$R_g \sim a N_D^{1/2} \left(\frac{N}{N_D}\right)^{1/3} \sim \frac{a^{4/3} N^{1/3}}{f^{1/3} l_B^{1/3}} \tag{11}$$

From this scaling relation, a globule can be envisioned as a closely packed assembly of $g = N/N_D$ Debye blobs, each containing N_D monomers and being of the size of the so-called Debye radius

$$R_D \sim a\sqrt{N_D} \tag{12}$$

Although such a picture conveys the correct scaling of the radius, it misrepresents the actual statistics of the PA chain, which is Gaussian over the full range of the globule radius R_g (and not only the Debye radius R_D); this fact will be of importance for the calculation of the spontaneous dipole moment of a PA globule in Appendix B. Neglecting contributions due to the globule surface, the free energy gain in the globular phase is roughly one k_BT per Debye blob. The total free energy in the globular state is therefore

$$F_g/k_BT \sim -N/N_D \tag{13}$$

In the discussion of the adsorption behavior so far we assumed that the charges are distributed randomly within the polyampholyte, leading to an average number of separated charges of $\tilde{Q} \sim (Nf)^{1/2}$. In Appendix B, we discuss the behavior of a collapsed polyampholyte in an external electric field. We find that the actual number of separated charges is drastically reduced in the globular state. Consequently, the tendency to adsorb is weakened. In principle, the adsorption on a charged surface can take two different routes: either the polyampholyte globule can be *dissolved* into a coil prior to adsorption (in which case the adsorption scenarios of the last sections would be valid), or the globule can adsorb *as a whole*. The actual adsorption scenario depends on which route gives a lower adsorption free energy.

We first discuss the adsorption energy of a globule as a whole. Using the result for the number of separated charges in a globule, $\tilde{Q}_g$, from Appendix B, eq B11, and the interaction energy between an oriented dipole and a charged plane, eq 3, we find

$$\frac{W_P}{k_BT} \simeq -\frac{\tilde{Q}_g R_g}{\lambda} \simeq -\frac{N^{1/2} a^2}{f^{1/2} l_B \lambda} \tag{14}$$

for a globule of radius R_g smaller than the Gouy–Chapman length λ, and

$$\frac{W_P}{k_BT} \simeq -\tilde{Q}_g \simeq -\frac{N^{1/6} a^{2/3}}{f^{1/6} l_B^{2/3}} \tag{15}$$

for a globule of radius R_g larger than the Gouy–Chapman length λ. The crossover between the two regimes occurs for $R_g \approx \lambda$, which, using eq 11, can be reexpressed as $f \approx Na^4/\lambda^3 l_B$. This boundary is drawn in Figure 3 as a broken line and is located in the adsorbed-globule region. The criterion for adsorption is obtained by comparing the globule-adsorption free energies in eqs 14 and 15 with unity. For small globules ($R_g < \lambda$) we thus obtain $f < a^4N/\lambda^2 l_B^2$ for adsorption to be possible, and for large globules ($R_g > \lambda$) the criterion for globule adsorption is $f < a^4N/\lambda^4$. We thus find a large region where adsorption of a globule as a whole is possible. We now have to check whether it is free-energetically advantageous to dissolve the globule and adsorb the PA in a coil state. To see this, we compare the free energies for the adsorbed coil states, eqs 9 and 7, with the free energy of the nonadsorbed globular state, eq 13; as turns out, the difference between the adsorbed and nonadsorbed globule free energies, eqs 14 and 15 and eq 13, respectively, is irrelevant for these phase boundaries. The pole regime is favored over the globular state for $f < a^4N/\lambda^2 l_B^2$, which determines the boundary between the pole and the desorbed-globule regimes (see Figure 3); this boundary is identical to the condition for the adsorption of whole small globules, and its extension thus separates the adsorbed and desorbed globule regimes. The fence regime is favored over adsorbed globules for $f < f_{ag} \equiv a^2/\lambda^{1/2} l_B^{3/2}$.

By combining all these phase boundaries, we obtain the phase diagram shown in Figure 3, which completely describes the adsorption behavior of neutral PA chains on charged surfaces in the absence of salt. There is a large region where globules are dissolved into uncollapsed blobs and adsorbed on the surface: this can be seen by extrapolating the boundary between the desorbed-coil and desorbed-globular regimes into the adsorbed coil phases. As the surface charge increases, the extent of the weakly adsorbed phase grows. At the threshold $\lambda \sim a^4/l_B^3$, the adsorbed globular phase disappears, and for $\lambda \sim a$, which corresponds to an extremely charged surface with charged groups separated less than the Bjerrum length, the fence and pole regions disappear (compare with Figure 2).

A word of caution is in order: the adsorption of a globule as a whole is a complex problem, because the adsorbed state results from a delicate balance of electrostatic interactions within the globule (leading to the globular state in the first place) and between charged monomers and the surface charges. For a constant external field, we could calculate the residual dipole moment of a globule within a simplified model (Appendix B). In this calculation we found no *soft* response (i.e., involving an interaction energy smaller than $1k_BT$) of the globule to the external field below the critical field strength necessary to completely dissolve the globule (see Appendix B). The application of this result to the present problem is straightforward for globules which are *smaller* than the Gouy–Chapman length: here, the external field is constant on the length scales of the globules. The case of globules which are larger than the Gouy–Chapman length is more complex, since the globules could undergo some conformational transformation to a slightly deformed globule or even to a state with an intermediate density between the globular and the coil state. This is beyond the scope of the present study. But we stress that changes (due to our oversimplified calculation) of the globule adsorption energy for globules larger than the Gouy–Chapman length would only concern the boundary between the adsorbed globular and adsorbed coil states, but would leave the boundaries to the nonadsorbed states unchanged.

C. Finite Salt Concentration. In all experimental aqueous systems there is a finite concentration of dissociated ions, which leads to a pronounced attenuation of electrostatic forces at large separations, referred

to as the screening effect. The potential of a charged surface in a salt solution of ion concentration c is given by[13]

$$\frac{eV_P(x)}{k_BT} = 2\ln\left(\frac{1-\gamma e^{-\kappa x}}{1+\gamma e^{-\kappa x}}\right) \tag{16}$$

where κ is the inverse screening length determined by

$$\kappa^2 = 4\pi l_B z^2 c$$

with z denoting the valency of the salt ions. The constant γ is determined by the electric surface field, which is proportional to the surface charge density σ

$$\frac{e}{k_BT}\frac{dV_P(x)}{dx}\bigg|_{x=0} = \frac{4\gamma\kappa}{1-\gamma^2} = \frac{e\sigma}{\epsilon\kappa_BT} = \frac{2}{\lambda}$$

The value of γ is

$$\gamma \approx \begin{cases} \dfrac{1}{2\lambda\kappa} & \text{for } \lambda\kappa \gg 1 \\ 1-\lambda\kappa & \text{for } \lambda\kappa \ll 1 \end{cases} \tag{17}$$

The first limit, $\lambda\kappa \gg 1$, corresponds to the Debye−Hückel regime, where the screening length is sufficiently short so that nonlinear effects can be neglected, the second limit is the Gouy−Chapman regime, where the Debye−Hückel approximation breaks down close to the charged surface. The surface potential reads

$$\frac{eV(0)}{k_BT} \approx \begin{cases} -\dfrac{2}{\lambda\kappa} & \text{for } \lambda\kappa \gg 1 \\ 2\ln\left(\dfrac{\lambda\kappa}{2}\right) & \text{for } \lambda\kappa \ll 1 \end{cases} \tag{18}$$

Noting that we set the potential at infinity to zero, one can easily see that the dimensionless potential at the surface is smaller than unity in the Debye-Hückel regime, but diverges logarithmically with the surface charge density and the screening length in the Gouy−Chapman limit. The asymptotic behavior of the potential is

$$\frac{eV(x)}{k_BT} \approx \begin{cases} -4\gamma e^{-\kappa x} & \text{for } \lambda\kappa \gg 1 \text{ or } x \gg \kappa^{-1} \\ 2\ln\left(\dfrac{\lambda\kappa}{2}\right) + 2\ln\left(1+\dfrac{x}{\lambda}\right) & \text{for } \lambda\kappa \ll 1 \text{ and } x \ll \kappa^{-1} \end{cases} \tag{19}$$

The interaction of the PA coil with the charged surface can be calculated similarly as for the salt-free case, given by eq 3, and reads

$$\frac{W_P}{k_BT} = -4\tilde{Q}\,\mathrm{arctanh}\left(\frac{\gamma e^{-\kappa z/2} - \gamma e^{-3\kappa z/2}}{1-\gamma^2 e^{-2\kappa z/2}}\right) \tag{20}$$

Again we need the asymptotic behavior of this interaction energy

$$\frac{W_P}{k_BT} \approx \begin{cases} -4\tilde{Q}\gamma e^{-\kappa z/2} & \text{for } z \gg \kappa^{-1} \\ -4\tilde{Q} & \text{for } \lambda < z < \kappa^{-1} \\ -4\tilde{Q}\,\mathrm{arctanh}\left(\dfrac{z}{2\lambda}\right) & \text{for } z < \kappa^{-1} \text{ and } z < \lambda \end{cases} \tag{21}$$

For a typical size z of the adsorbed PA smaller than the screening length, there is no influence of the salt. For a typical size larger than the screening length, the screening of the electrostatic field becomes relevant.

Let us first discuss the case of small salt concentration when the screening length is larger than the Gouy−Chapman length (leading, inter alia, to $\gamma \approx 1$), i.e., $\kappa^{-1} > \lambda$. Since the electrostatic interaction is not changed on length scales smaller than the screening length, the fence and the pole regimes are not affected by the salt. The weakly adsorbed regime is only affected for a vertical size larger than the screening length, i.e. for $R_z \sim a/f^{1/2} > \kappa^{-1}$. Let us consider a Gaussian subchain of length N with a vertical size $z \sim aN^{1/2}$ and uncompensated charges of magnitude $\tilde{Q} \sim (fN)^{1/2}$. Using eq 21 the interaction energy can be rewritten as $W_P/k_BT \sim -(fN)^{1/2}\exp(-[a\kappa/f^{1/2}](fN)^{1/2})$. Since the factor $[a\kappa/f^{1/2}]$ in the exponential is larger than one, it is clear that the electrostatic attraction is actually never larger than unity, so that weak adsorption is impossible if the blob size is larger than the screening length or if $f < f_{sw} \equiv a^2\kappa^2$. This is depicted in Figure 4a. The corresponding monomer number is $N_s \equiv 1/a^2\kappa^2$. As has been shown by Higgs and Joanny,[3] the formation of globules is affected if $R_D > \kappa^{-1}$. Under such high-salt conditions, globules form only if the monomer number is larger than $N_{Ds} \equiv N_D{}^2\kappa^2a^2$ or, equivalently, for $f > a^{3/2}\kappa^{1/2}/l_BN^{1/4}$. The radius of such a salty globule is given by $R_{gs} \sim aN^{1/3}N_{Ds}{}^{1/6}$. Salty globules are always larger than the screening length, so that the interaction energy with the charged surface can be neglected, by the same arguments as used for the adsorption of Gaussian chains given above. Salty globules are therefore always desorbed. The minimal monomer number in order to observe salty desorbed globules is $N_{sg1} \equiv l_B{}^4\kappa^6a^2$, as shown in Figure 4a.

For intermediate salt concentrations, for $\lambda > \kappa^{-1} > \lambda^{2/3}l_B{}^{1/3}$, the weakly adsorbed regime has disappeared, as depicted schematically in Figure 4b. The vertical height of the salty fence is reduced to $R_z \sim \kappa^{-1}$. The minimal charge fraction in order to observe the salty fence is $f_{sf} \equiv \kappa^4a^2\lambda^2$. Comparing the free energy of the salty fence with that of a normal (salt-free) globule, one finds that the globule is dissolved and adsorbed for $f < f_{sag} \equiv a^2/\lambda\kappa^{1/2}l_B{}^{3/2}$, which is smaller than in the salt-free case. The adsorbed globule phase is not affected by the salt, since at the boundary to the desorbed globule phase the size of the globules is smaller than the screening length. The minimal monomer number in order to observe salty desorbed globules is $N_{sg2} \equiv l_B{}^4\kappa^{14}\lambda^8a^2$.

Finally, all adsorption disappears if the screening length becomes even smaller, i.e., for $\lambda^{2/3}l_B{}^{1/3} > \kappa^{-1}$. As demonstrated in Figure 4c, the desorbed salty globules transform into desorbed (normal) globules for $f > f_{dg} \equiv a^2\kappa/l_B$.

The various crossover scales appearing in the phase diagrams presented in Figures 3 and 4 are summarized in Table 1.

D. Polyampholytes with a Net Charge. Polyampholytes with a nonvanishing net charge have been studied in detail, and there is an interesting crossover from a pure PA behavior, dominated by attraction between unlike charges, to a PE behavior, dominated by repulsion between similarly charged monomers.[14−16] This crossover can be understood by introducing the electrostatic blobsize $N_{el} \equiv (a/l_B\Delta f^2)^{2/3}$, which is the monomer number at which the electrostatic repulsion energy reaches k_BT. For $N < N_{el}$ the polymer chain is

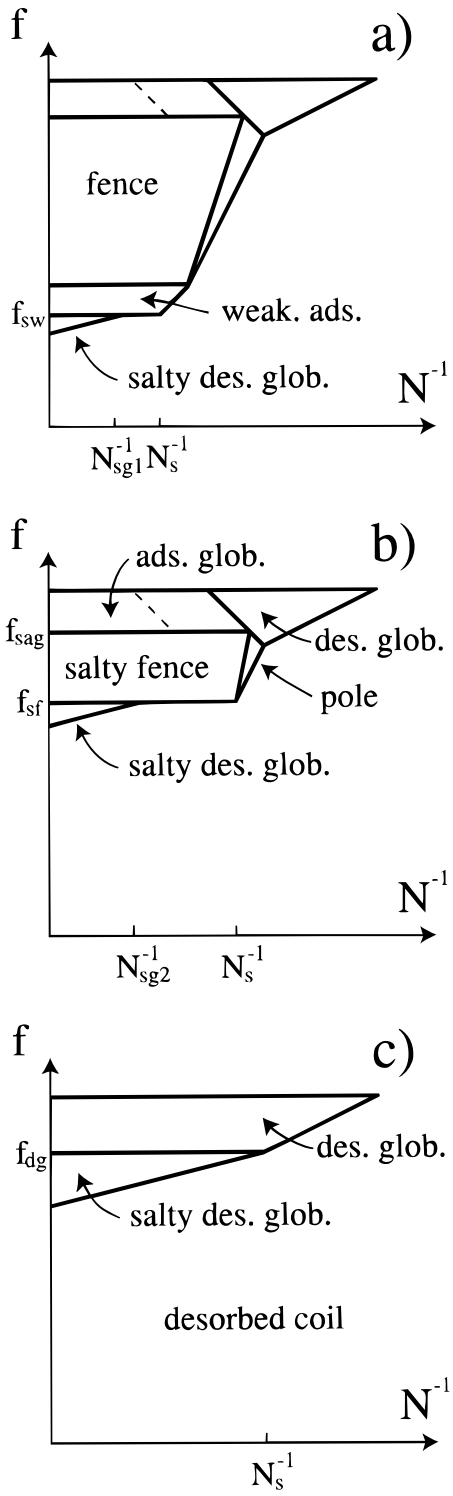

Figure 4. Adsorption of a neutral PA on a charged surface in the presence of salt. (a) For small salt concentration, $\kappa^{-1} > \lambda$, the strong and globular adsorption regimes are not affected by the salt and the upper part of the phase diagram is the same as Figure 3. The weak adsorption regime is eliminated for $f < f_{sw} = a^2\kappa^2$, and one observes a transition to a salty globule for a minimal monomer number of $N_{sg1} = l_B^4\kappa^6a^2$. (b) Phase diagram for intermediate salt concentration, for $\lambda > \kappa^{-1} > \lambda^{2/3}l_B^{1/3}$. The desorbed-coil/desorbed-globule boundary is not affected, but the transition from the pole to the fence regime is shifted upwards and the fence/adsorbed globule boundary is shifted downward, thus diminishing the fence regime from the top and the bottom. (c) Phase diagram valid for $\lambda^{2/3}l_B^{1/3} > \kappa^{-1}$. All adsorbed phases have disappeared, and the only transition occurs between salty and normal globules at $f_{dg} = a^2\kappa/l_B$.

Table 1. Scaling Boundaries for the Adsorption on a Charged Plane (Compare with Figures 3 and 4)

	No Salt	
f_f	a^2/λ^2	fence regime
f_{ag}	$a^2/\lambda^{1/2}l_B^{3/2}$	adsorbed globules
N_{dg}	a^2/l_B^2	desorbed globules
N_p	$\lambda^{4/3}l_B^{2/3}/a^2$	pole regime
N_{wa}	λ^2/a^2	weakly adsorbed
	With Salt	
f_{sw}	$a^2\kappa^2$	salty weakly adsorbed
f_{sf}	$a^2\kappa^4\lambda^2$	salty fence
f_{sag}	$a^2/\lambda\kappa^{1/2}l_B^{3/2}$	salty adsorbed globule
f_{dg}	$a^2\kappa/l_B$	desorbed (normal) globule
N_s	$a^{-2}\kappa^{-2}$	salt dominated
N_{sg1}	$l_B^4\kappa^6a^2$	salty (desorbed) globule 1
N_{sg2}	$l_B^4\kappa^{14}\lambda^8a^2$	salty (desorbed) globule 2

Gaussian; for $N > N_{el}$, it takes a rod-like configuration and thus behaves like a polyelectrolyte (PE). The formation of PA globules is inhibited if $N_{el} < N_D$, i.e., for $f < f_n \equiv (a\Delta f/l_B)^{2/3}$. A more subtle aspect concerns a configurational change of a globule, which is expected to occur when the electrostatic repulsion pressure (obtained from the electrostatic energy $W_{el}/k_BT \sim l_B\Delta f^2N^2/R_g$ by taking a derivative with respect to the globule radius R_g) equals the Laplace pressure (obtained from the surface energy $W_{surf}/k_BT \sim R_g^2/a^2N_D$); this happens at $f \sim N\Delta f^2$. More detailed calculations show that the globule then actually forms a necklace of smaller globules. The resulting phase diagram is shown in Figure 5a and is equivalent to Figure 1 of ref 11. This phase diagram remains valid for small salt concentrations as long as the electrostatic blob radius is smaller than the screening length, i.e. for $R_{el} \sim aN_{el}^{1/2} < \kappa^{-1}$, or, equivalently, for $\Delta f > a^2\kappa^{3/2}/l_B^{1/2}$. The only effects of the salt in this case is to introduce a finite persistence length in the PE and necklace-globule regimes.

For higher salt concentrations, corresponding to the condition $\Delta f < a^2\kappa^{3/2}/l_B^{1/2}$, the phase behavior is more complicated. The electrostatic self-energy of a charged coil which is larger than the screening length is given by $W_{el}/k_BT \sim l_B\Delta f^2N^2/R^3\kappa^2$. By setting this energy equal to unity, we obtain the salty electrostatic blob size as $N_{sel} \equiv a^6\kappa^4/l_B^2\Delta f^4$. For shorter chains, the polymer remains Gaussian; for longer chains, the polymer is isotropically swollen. The transition from this swollen regime to the salty globule is obtained by equating the salty electrostatic blob size with the salty Debye size, $N_{sel} \sim N_{Ds}$, which yields $f_{sg} \sim \Delta f/(l_B\kappa)^{1/2}$. The electrostatic repulsion within the salty and normal globules is always weaker than the attraction between unlike charges and a necklace regime does not occur. The resulting phase diagram is plotted in Figure 5b which is in its upper part identical to the one shown in Figure 4c. The various crossover scales occuring for the case of charged PA are summarized in Table 2.

After having clarified the PE/PA scaling regimes in the presence of salt, we now consider the adsorption behavior on a charged surface. We concentrate on the case where the PA has a net charge $\Delta f\,N$ of the same sign as the surface (adsorption of a polyelectrolyte chain with a net charge of different sign than the surface has been treated in ref 17). In the absence of salt, the electrostatic energy to bring a charged PA from infinity towards the surface is infinite, and adsorption cannot occur. It is therefore clear that salt is necessary for adsorption and plays a decisive role.

We first investigate the case of large salt concentration, i.e., small screening length, $\kappa^{-1} < \lambda$. The screening

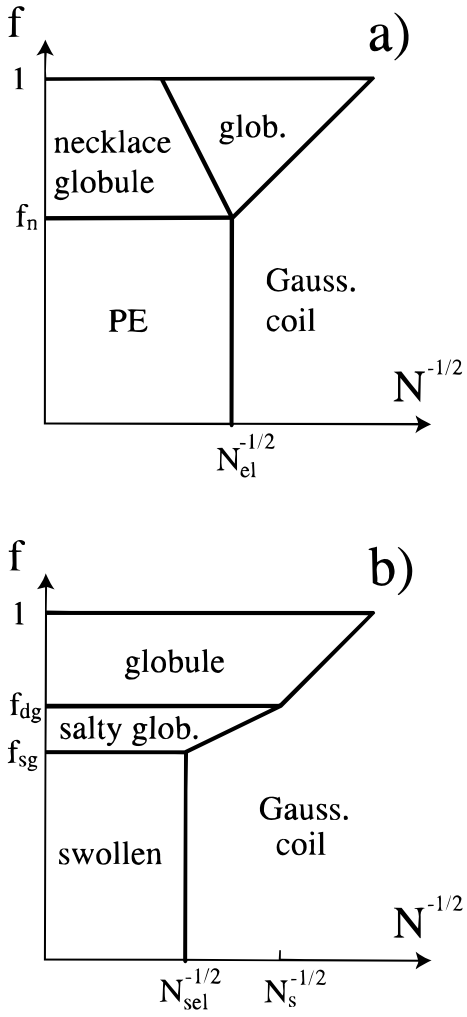

Figure 5. (a) Phase diagram for a PA chain at low salt concentration or relatively large net charge fraction, $\Delta f > a^2\kappa^{3/2}/l_B^{1/2}$, for which case the electrostatic blob size $R_{el} \sim aN_{el}^{1/2}$ is smaller than the screening length κ^{-1}. The polymer is in a stretched polyelectrolyte (PE) configuration for long chains $N > N_{el} \equiv (a/l_B\Delta f^2)^{2/3}$ (with a persistence length which depends on the salt concentration), and the globular phase transforms into a necklace structure when the electrostatic pressure exceeds the Laplace surface tension, i.e., for $f < N\Delta f^2$. The transition between the polyelectrolyte and the necklace globule regime occurs when the electrostatic blobsize, N_{el}, equals the Debye blob size, N_D, for $f \sim f_n \equiv (a\Delta f/l_B)^{2/3}$. (b) Phase diagram for a PA chain at high salt concentration or relatively small net charge fraction, $\Delta f < a^2\kappa^{3/2}/l_B^{1/2}$, such that the electrostatic blobsize is larger than the screening length, $R_{el} \sim aN_{el}^{1/2} > \kappa^{-1}$. Here the net charge leads to an isotropically swollen configuration for long enough chains, $N > N_{sel}$; i.e., the electrostatic repulsion is weak for large separations and cannot stretch the PA chain. The globule occurs in a salty version for intermediate values of the charged-monomer fraction $f_{sg} < f < f_{dg}$, and the necklace formation is inhibited.

Table 2. Scaling Boundaries for Polyampholytes with a Net Charge in the Presence of Salt (Compare with Figure 5)

f_n	$(a\Delta f/l_B)^{2/3}$	necklace globule
f_{sg}	$\Delta f/l_B^{1/2}\kappa^{1/2}$	salty (desorbed) globule
N_{el}	$(a/l_B\Delta f^2)^{2/3}$	electrostatic blob size
N_{sel}	$a^6\kappa^4/l_B^2\Delta f^4$	salty electrostatic blob size

length cannot become arbitrarily large, since for $\kappa^{-1} < \lambda^{2/3}l_B^{1/3}$ no adsorption is possible at all, even if the PA chain is neutral (compare with Figure 4c). We are therefore interested in modifications of the phase diagram in Figure 4b due to net charge effects. Using eq 19 from the last section, the repulsion due to the net charge is

$$\frac{W_{rP}}{k_BT} \simeq \frac{2\Delta fN}{\lambda\kappa}e^{-\kappa z/2} \tag{22}$$

As we obtained in section II.C, the main effect of added salt is to limit the vertical size of the adsorbed chain to the screening length, and we can write the repulsion energy as

$$\frac{W_{rP}}{k_BT} \simeq \frac{\Delta fN}{\lambda\kappa} \tag{23}$$

In order to obtain the adsorption behavior of the charged PA, we compare the free energy of the single coil phase, eq 7, with the repulsive energy eq 23, and obtain the single-coil adsorption to be possible only for $f > \Delta f\lambda/a^2\kappa N$. We obtain the following succession of changes to the phase diagram in Figure 4b.

(i) For $\Delta f < a^2\kappa^3\lambda$, the salty fence regime is unchanged, and for $N > N_{sel}$, the desorbed coil state goes over into the isotropically swollen desorbed phase (compare with Figure 5b). (ii) For $a^2\kappa^3\lambda < \Delta f < a^2\kappa^{3/2}/l_B^{1/2}$, the salty fence regime is reduced due to the net charge, and only occurs in the range $\Delta f^{3/2}\lambda^{1/2}/a\kappa^{1/2} < f < f_{sag} \equiv a^2/l_B^{3/2}\kappa^{1/2}\lambda$. We still find an adsorbed globule regime. Figure 5b still describes the chain behavior for the desorbed phases.

(iii) For larger values of Δf, i.e. $\Delta f > a^2\kappa^{3/2}/l_B^{1/2}$, the adsorbed globule regime vanishes. Now the desorbed regimes are described by Figure 5a, and the desorbed chain is therefore in a stretched PE state for $N > N_{el}$. Still, the salty fence exists in the range $\Delta f^{3/2}\lambda^{1/2}/a\kappa^{1/2} < f < f_{sag}$. The salty fence regime persists until the net charge fraction reaches the value $\Delta f \sim a^2/l_B\lambda$, above which value no adsorption is possible for any values of the other parameters.

In the opposite limit, for small salt concentrations and large screening length, $\kappa^{-1} > \lambda$, the electrostatic repulsion is, according to eq 19

$$\frac{W_{rP}}{k_BT} \simeq -2\Delta fN\left[\ln\left(\frac{\lambda\kappa}{2}\right) + \ln\left(1 + \frac{z}{2\lambda}\right)\right] \tag{24}$$

where z is the distance of the PA chain from the surface. In this case we are interested in changes from Figure 4a due to the net charge. Since the maximal vertical size of the adsorbed chain is the screening length (realized for the weakly adsorbed phase, compare Figure 4a), the constant term in the interaction dominates the repulsion, so the repulsion energy can be rewritten as

$$\frac{W_{rP}}{k_BT} \sim \Delta f\, N \ln(1/\lambda\kappa) \tag{25}$$

Enforcing the repulsive energy due to the net charge to be smaller than the attractive gain due the PA−dipole field interaction, we arrive at the following critical net charge fractions: The weakly adsorbed regime is totally eliminated for $\Delta f \ln(1/\lambda\kappa) > a^2/\lambda^2$. Adsorbed globules disappear for $\Delta f \ln(1/\lambda\kappa) > a^2/\lambda^2(\lambda/l_B)^{1/2}$. For $\Delta f \ln(1/\lambda\kappa) > a^2/\lambda l_B$, no adsorption is possible for any values of the other parameters. As could be expected, the maximal net charge that can be adsorbed is smaller than in the high-salt-concentration case.

We obtain the contra-intuitive result that in order to adsorb a PA with a net charge of the same sign as the

surface, the surface has to be quite strongly charged; i.e., the Gouy−Chapman length has to be small. The other result is that the adsorption of a PA with the same charge as the wall is possible only if salt is present. Note however that if the salt concentration is small ($\kappa\lambda < 1$), the effect of salt comes only into logarithmic factors which vary only very weakly.

III. Polyampholytes at Charged Cylinders

A charged cylinder of radius R is characterized by its charge per unit length, τ, or by the dimensionless charge parameter $\tilde{\tau} = \tau l_B/e = \tau e/(4\pi\epsilon k_B T)$, which is a measure of its charge strength. In contrast to the case of a charged plane, a charged cylinder in the absence of any confining outer walls is not able to bind all of its counterions. As turns out in a mean-field treatment (which is recalled in Appendix A), the interaction between a charged cylinder and its counterions is irrelevant for $\tilde{\tau} < 1$: The counterions are delocalized, and the counterion density goes to zero as the system size diverges. For $\tilde{\tau} > 1$, there is a finite fraction $(\tilde{\tau} - 1)/\tilde{\tau}$ of counterions loosely bound to the cylinder, and the effective charge of the combined cylinder−counterion system approaches $\tilde{\tau} \to 1$ as one goes far away from the cylinder: This phenomenon is called charge renormalization. It is important to note that in the latter case the counterions are not bound directly at the cylinder surface, but form a rather loose cloud around the cylinder. The distinctive change of the counterion density distribution above and below $\tilde{\tau}$ is associated with a phase transition, which is called the *Manning transition*.[18]

Below the Manning threshold, i.e., for $\tilde{\tau} < 1$, the electrostatic potential around a cylinder of radius R equals the bare potential in the absence of counterions

$$\frac{eV_C(x)}{k_B T} = 2\tilde{\tau} \ln(1 + x/R) \tag{26}$$

where $x = r - R$ measures the distance from the cylinder surface. Neglecting the curvature effect of the cylindrical geometry, which should be a good approximation for stretched polyampholytes coils which are not larger than the cylinder radius, the free energy expression has exactly the same form as for the planar case, eq 4

$$\frac{F_C}{k_B T} = \frac{z^2}{a^2 N} - 4(fN)^{1/2}\tilde{\tau} \operatorname{arctanh}\left(\frac{z}{2R}\right) \tag{27}$$

provided that λ is replaced by R and $f^{1/2}$ by $f^{1/2}\tilde{\tau}$. The discussion is exactly the same as in section II. The resulting different adsorption regimes are described by Figures 3 and 4 if one identifies the vertical phase-diagram coordinate as $f\tilde{\tau}^2$. Since the fraction of charged monomers also enters the calculation via the Debye monomer number N_D, eq 10, we have to rescale the Bjerrum length and replace l_B by $l_B/\tilde{\tau}^2$ in all expressions. We obtain the following results: in the strong adsorption (or fence) regime, the PA coil is adsorbed in a layer of the width of the cylinder radius R. The upper boundary of all phase diagrams is $f\tilde{\tau}^2 = \tilde{\tau}^2$ and corresponds to a fully charged PA, $f = 1$. For a cylinder charge smaller than $\tilde{\tau} < (l_B/R)^{1/2}$ the fence regime disappears and a transition between the adsorbed globule phase and the weakly adsorbed phase remains at $f\tilde{\tau}^2 \sim a^2\tilde{\tau}^4/l_B^2$. The resulting phase behavior for infinitely long chains is shown in Figure 6a as a function of the cylinder radius R.

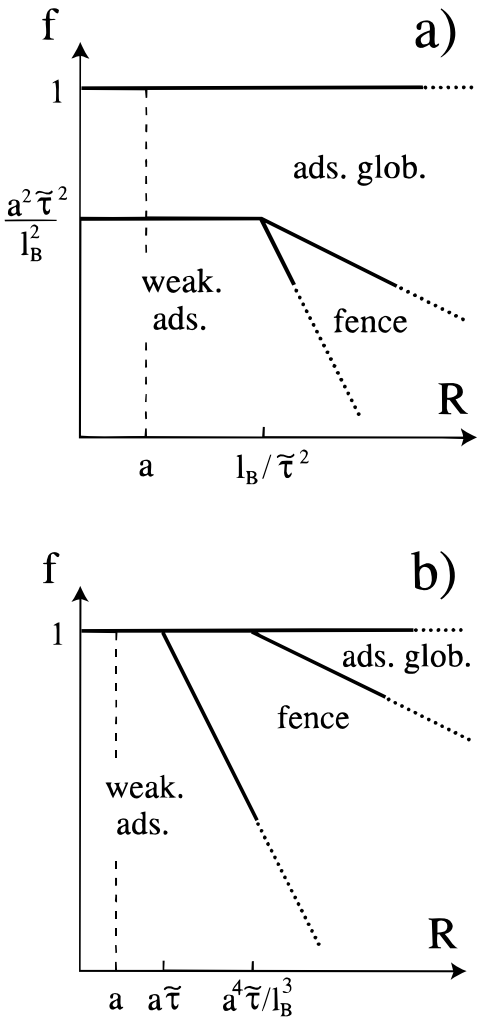

Figure 6. Adsorption phase diagram of a neutral PA chain on a charged cylinder of radius R in the limit of an infinitely long polymer (a) below the Manning threshold, $\tilde{\tau} < 1$, and (b) above the Manning threshold, $\tilde{\tau} > 1$. The case corresponding to a PA complexation on a polyelectrolyte, $R \sim a$, is denoted by broken lines.

Above the Manning condensation threshold, i.e., for a charge parameter $\tilde{\tau} > 1$, the potential distribution shows a pronounced crossover behavior (see Appendix A). For distances from the cylinder surface smaller than the cylinder radius, one finds

$$\frac{eV_C(x)}{k_B T} = 2 \ln(1 + \tilde{\tau}x/R) \tag{28}$$

which is identical to the potential obtained in the planar geometry, eq 1, given that one defines a cylindrical Gouy−Chapman length $\lambda_c \equiv R/\tilde{\tau}$. One notes that the cylindrical Gouy−Chapman length follows from the standard definition eq 2 if one uses as the surface charge density the cylindrical analogue $\sigma_C = \tau/2\pi R$. Since we are discussing the case $\tilde{\tau} > 1$, the cylindrical Gouy Chapman length is always smaller than the radius; the approximation in eq 28 is therefore well justified as long as x is not larger than the cylindrical Gouy Chapman length λ_C; this condition is satisfied in the single-coil and strong-adsorption regimes. For distances larger than the radius one finds a potential corresponding to

a charge parameter of $\tilde{\tau} = 1$ (see Appendix A), which however only applies to very thick layers of adsorbed PA in the weak-adsorption regime, where we expect curvature effects to become important. For $\tilde{\tau} > 1$, one can thus use the results obtained for the adsorption on a planar surface if one uses the cylindrical Gouy−Chapman length λ_c in all expressions. For strongly charged cylinders, the PA in the strong-adsorption regime is adsorbed in a layer of thickness given by the cylindrical Gouy−Chapman length, which is smaller than the cylinder radius. The resulting phase behavior for infinitely long chains is shown in Figure 6b as a function of the cylinder radius R.

Of particular interest is the case where the polyampholyte adsorbs on a cylinder with a diameter of the order of the monomer size a, which would schematically correspond to the complexation of a rigid polyelectrolyte by a polyampholyte. This case is indicated by a broken line in parts a and b of Figure 6. In this case no strong adsorption can occur. If the polyelectrolyte is below the Manning condensation threshold (Figure 6a), the adsorption can occur in the weak adsorption regime with a diameter of the complex of $R_z \propto a/f^{1/2}$ if $f\tilde{\tau}^2 > 1/N$ and $f\tilde{\tau}^2 < a^2\tilde{\tau}^4/l_B^2$. If in fact $N > N_D$, this corresponds to the dissolution of a PA globule. For $f\tilde{\tau}^2 > a^2\tilde{\tau}^4/l_B^2$, the globule adsorbs as a whole for a long enough chain, i.e., $f\tilde{\tau}^2 < Na^2\tilde{\tau}^4/l_B$. If the polyelectrolyte is above the Manning condensation threshold (Figure 6b), complexation always occurs in the weak adsorption regime, i.e., globules are always dissolved. The transverse size of the complex is $R_z \propto a/f^{1/2}$. Note that in this case the Gouy Chapman length is smaller than the typical size a of the charges and that the excluded volume of the charges that has been ignored could play an important role.

The longitudinal size L of the polyampholyte (along the cylindrical polyampholyte) is obtained from a Flory argument by estimating directly the electrostatic free energy. Below the condensation threshold, $L = N(f\tilde{\tau})^{2/3}a$ and above the threshold $L = Nf^{2/3}a$.

IV. Polyampholytes at Charged Spheres

The adsorption of polyampholytes on charged spheres deviates in two points from that on planar surfaces and cylinders:

(i) A sphere has a finite surface area, and interactions between adsorbed PA blobs become important for long enough polyampholytes. This leads to multilayer adsorption and other interesting effects, as will be discussed in section IV.B.

(ii) An isolated sphere is not able to bind its counterions, unless it is enclosed in a finite box. For isolated spheres the counterions can therefore be neglected. For a solution with a finite concentration of spheres, the necessarily finite counterion concentration is taken into account by introducing a finite screening length, quite similarly to the addition of salt; this is discussed in details in section IV.C. For strongly charged spheres, a nonlinear condensation of the counterions around the spheres occurs which has has been described in terms of a renormalized charge of the sphere;[19] this is however beyond the scope of the present paper.

The bare potential (in the absence of salt and counterions) of a sphere of charge Z and radius R is

$$\frac{eV_S(x)}{k_BT} = \frac{Ze^2}{4\pi\epsilon k_BT}\frac{1}{R+x} = \frac{Zl_B}{R+x} \tag{29}$$

where x measures the distance to the sphere surface. The electrostatic energy of a polyampholyte chain with $\tilde{Q}$ separated charge units at a charged sphere is, using the same geometry as depicted in Figure 1

$$\frac{W_S}{k_BT} = Zl_B\tilde{Q}\left[\frac{1}{R+z_0+z/2} - \frac{1}{R+z_0-z/2}\right] = -Zl_B\tilde{Q}\frac{z}{(R+z_0)^2 - z^2/4} \tag{30}$$

For the charged sphere, the effect of the electrostatic potential on the PA chain is different from the charged surface or cylinder. Here, the electrostatic energy W_S possesses a minimum at a chain size z approximately equal to the sphere radius R. The electrostatic interaction stretches the chain for small coil radii, $z < R$, and compresses it for larger radii, $z > R$. Note, however, that this is due to our oversimplified symmetric dumbbell model for the polyampholyte chain. In a more refined model where the two charged halves of the polyampholyte chain have different sizes, the electrostatic free energy is monotonously decreasing. As the final results of our analysis are not affected by this minimum in the energy (the PA chain avoids compression by forming multiple blobs), we proceed with this simple model despite its artifacts. A detailed description of the conformation of an adsorbed polyampholyte is extremely complex and is far beyond the scope of this work.

The elastic deformation of the PA chain in the electrostatic potential is associated with an elastic energy. For a PA chain in the coil state (below the globulization threshold), the number of separated charges is of the order $\tilde{Q} \sim (fN)^{1/2}$, and the resulting free energy can be written as

$$\frac{F_S}{k_BT} \sim \begin{cases} \dfrac{z^2}{a^2N} - z\dfrac{Zl_B\sqrt{fN}}{R^2} & \text{for } z < R \\ \dfrac{a^2N}{z^2} - \dfrac{Zl_B\sqrt{fN}}{z} & \text{for } z > R \end{cases} \tag{31}$$

Introducing rescaled variables for the sphere charge

$$\tilde{Z} \equiv \sqrt{f}Z\frac{l_B}{a} \tag{32}$$

and for the sphere radius

$$\tilde{R} \equiv \frac{R}{a\sqrt{N}} \tag{33}$$

the chain radii, obtained by minimizing the free energy expression eq 31, can be written as

$$z \sim \begin{cases} a\sqrt{N}\,\dfrac{\tilde{Z}}{R^2} & \text{for } z < R \rightarrow \tilde{Z} < \tilde{R}^3 \\ a\sqrt{N} & \text{for } z \approx R \rightarrow \tilde{Z} > \tilde{R}^3 \text{ and } \tilde{Z} > 1/\tilde{R} \\ a\sqrt{N}\,\dfrac{1}{\tilde{Z}} & \text{for } z > R \rightarrow \tilde{Z} < 1/\tilde{R} \end{cases} \tag{34}$$

In between the regimes where the chain is highly stretched or compressed, the coil is relaxed and has a typical size of the order of the Gaussian radius of gyration. The stretched solution, for $z < R$, is of course only valid for $z > aN^{1/2}$, or, equivalently, for $\tilde{Z} > \tilde{R}^2$. For $\tilde{Z} < \tilde{R}^2$ the relaxed solution, $z \approx aN^{1/2}$, is realized.

Conversely, the compressed solution is only valid for $z < aN^{1/2}$, or $\tilde{Z} > 1$. Again, for $\tilde{Z} < 1$, the relaxed solution, $z \sim aN^{1/2}$, is realized.

The free energies for the three different solutions are

$$\frac{F_S}{k_B T} \sim \begin{cases} -\dfrac{a^2 Z^2 l_B{}^2 f N^2}{R^4} \sim -\dfrac{\tilde{Z}^2}{\tilde{R}^4}, \text{ stretched, } \tilde{R}^2 < \tilde{Z} < \tilde{R}^3 \\ -\dfrac{Z l_B \sqrt{fN}}{R} \sim -\dfrac{\tilde{Z}}{\tilde{R}}, z \approx R, \tilde{R}^3 < \tilde{Z} \text{ and } 1/\tilde{R} < \tilde{Z} \\ -\dfrac{Z^2 l_B{}^2 f}{a^2} \sim -\tilde{Z}^2, \text{ compressed, } 1 < \tilde{Z} < 1/\tilde{R} \end{cases} \quad (35)$$

The free energy of the relaxed state with a coil size $z \approx R$ matches continuously with the free energy of the deformed states at the boundaries, $\tilde{Z} \sim \tilde{R}^3$ and $\tilde{Z} \sim 1/\tilde{R}$, as expected. At the onset of the stretched state, for $\tilde{Z} \sim \tilde{R}^2$ or $f \sim a^2\tilde{R}^4/l_B{}^2Z^2$, the adsorption free energy of the stretched coil is 1 k_BT. This boundary therefore also denotes the adsorption threshold, i.e., the boundary between the desorbed-coil and the single-blob or pole regimes.

The functional dependence of the free energies on N suggests the formation of blobs, for the same reasons as in the previous sections on charged surfaces and cylinders. Blob formation sets in at the threshold between the stretched and relaxed coil conformations, which occurs for $\tilde{Z} \sim \tilde{R}^2$ or $f \sim a^2\tilde{R}^6/l_B{}^2Z^2$. This denotes the boundary between the pole and fence regimes. The free energy per blob follows from eq 35 to be $F_b/k_BT \sim -\tilde{Z}^{2/3}$, and the number of monomers in a blob is $N_b \sim \tilde{Z}^{-2/3}R^2/a^2$. The free energy of the adsorbed polymer consisting of $g = N/N_b$ blobs is therefore

$$\frac{F_S}{k_B T} \sim \frac{N}{N_b}(1 - \tilde{Z}^{2/3}) \quad (36)$$

The formation of a fence is only favorable if the adsorption free energy F_S/k_BT is negative. The fence regime is therefore realized for $\tilde{Z} > \tilde{R}^3$ and $\tilde{Z} > 1$, or, equivalently, $f > a^2\tilde{R}^6/l_B{}^2Z^2$ and $f > f_f^s \equiv a^2/l_B{}^2Z^2$. The thickness of the adsorbed layer is of the order of the sphere radius R. In contrast to the case of the planar surface or cylinder we do not find a weakly adsorbed polymer layer. This has to do with the fact that the electrostatic adsorption potential for the sphere, eq 30, goes to zero for large coils, whereas it approaches a constant for the plane and the cylinder; compare with eq 3.

A. Adsorption of Polyampholyte Globules. For the adsorption of a PA globule we have again the two alternative routes already encountered for the planar case: the globule can adsorb as a whole, or it can be dissolved and adsorbed in a coillike state. Let us consider first the adsorption as an intact globule. For a globule radius R_g smaller than the sphere radius R, we can use the asymptotic form of eq 30 for small separations and obtain the electrostatic gain in the adsorbed state as

$$\frac{W_S}{k_B T} \sim -Z l_B \tilde{Q}_g R_g/R^2 \sim -\frac{Z_*^2}{\tilde{R}\tilde{Z}} \quad (37)$$

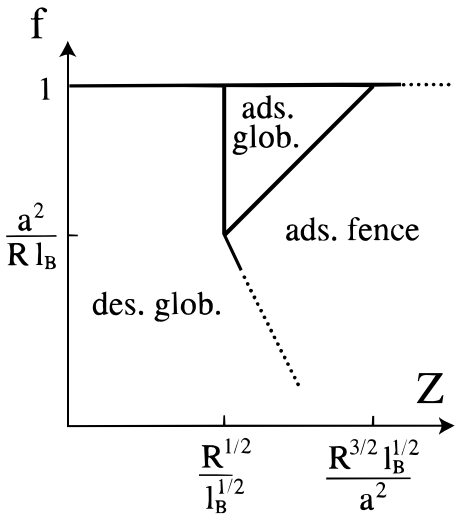

Figure 7. Phase diagram for the adsorption of a neutral PA chain on a sphere of charge Z in the limit of an infinitely long polymer. Adsorption only occurs for a sphere charge larger than $Z \sim R^{1/2}/l_B{}^{1/2}$.

where the globule radius, R_g, is given by eq 11 and the number of uncompensated charges in a globule, $\tilde{Q}_g$, by eq B11. We have used the rescaled parameter

$$Z_* \equiv \sqrt{\frac{l_B}{R}}Z \quad (38)$$

which together with $\tilde{Z}$ (which is used to express the f-dependence) and $\tilde{R}$ (which contains the N-dependence) conveniently describes the PA adsorption on spheres. In the opposite limit, for a globule radius larger than the sphere radius, we obtain an electrostatic adsorption energy of

$$\frac{W_S}{k_B T} \sim -Z l_B Q_g/R_g \sim -(\tilde{Z}\tilde{R}Z_*{}^2)^{1/3} \quad (39)$$

The globule radius is smaller than the sphere radius only for $\tilde{Z} > Z_*/\tilde{R}$. Defining the adsorption threshold by $W_S/k_BT = -1$ as we did in the previous sections, we see that globule adsorption is possible in the parameter range $1/\tilde{R}Z_*{}^2 < \tilde{Z} < Z_*{}^2/R$, which shrinks to zero as $Z_* \to 1$. It follows that globule adsorption only occurs for $Z_* > 1$.

In order to decide whether a globule is dissolved prior to being adsorbed, we need to compare the free energy of the globule, eq 13, with the adsorbed coil states, eqs 36 and 35. For the fence regime, the dissolution of the globule is favorable for

$$\tilde{Z} < Z_*{}^{3/2} \quad (40)$$

or, equivalently, $f < f_{ag}^s \equiv Za^2/l_B{}^{1/2}R^{3/2}$. A similar comparison with the free energy of the adsorbed single coil (in the pole regime) leads to globule dissolution for

$$\tilde{Z} < Z_*{}^2/\tilde{R} \quad (41)$$

which coincides with the adsorption threshold for small globules, eq 37. The resulting phase behavior for infinitely long chains is depicted in Figure 7 as a function of the sphere charge Z and the charged-monomer fraction f. The most striking feature is that PA adsorption is possible only for a sphere charge larger

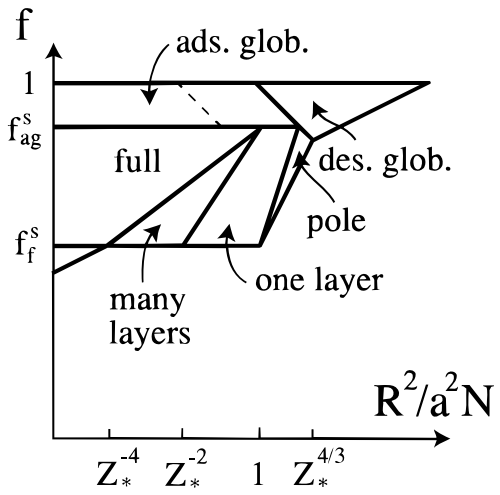

Figure 8. Phase diagram for the adsorption of a neutral PA chain on a sphere of radius R and intermediate charge, $R^{1/2}/l_B^{1/2} < Z < R^{3/2}l_B^{1/2}/a^2$. The adsorbed coil states are divided into the single-coil or pole state, the phase of one incomplete layer, the phase of one (or more) complete layers, and a region where the sphere is full and the adsorbed PA portion coexists with a non-adsorbed globular portion. The weakly adsorbed regime seen for adsorption on planes and cylinders is absent, and the desorbed globular regime occurs above and below the adsorbed phases. Globules can either adsorb as a whole, or be dissolved prior to adsorption.

than $Z > (R/l_B)^{1/2}$ (equivalent to the condition $Z_* > 1$). From eq 36 the fence regime only occurs for $\tilde{Z} > 1$, from which one obtains the boundary between the fence and the desorbed globule regime, $f^s_f \equiv a^2/l_B{}^2Z^2$. The transition from the adsorbed-globule to the fence regime is obtained from eq 40 as $f^s_{ag} \equiv Za^2/l_B{}^{1/2}R^{3/2}$.

In Figure 8 we show the adsorption behavior for finite chains and for an intermediate sphere charge $(R/l_B)^{1/2} < Z < R^{3/2}l_B{}^{1/2}/a^2$ as a function of the charged-monomer fraction f and the rescaled inverse monomer number R^2/a^2N. For this range of sphere charges, we obtain the sequence of adsorbed-globular, fence, and desorbed-globular regimes for long polymers (to the left in Figure 8). In addition, the results of the following section are shown, which demonstrate the effect of the overfilling of the sphere surface with adsorbed PA and further subdivide the fence regime into a one-layer regime, a many-layers regime, and a full regime. As Z decreases, the extent of the fence regime shrinks, and the remaining adsorbed-globular regime disappears for $Z \sim (R/l_B)^{1/2}$ (or $Z_* \sim 1$). For increasing sphere charge, the adsorbed-globule phase disappears at $Z \sim R^{3/2}l_B{}^{1/2}/a^2$ (as explicitly demonstrated in Figure 7). We also show in the phase diagram the line on which the globule size equals the sphere radius (broken line), which is embedded in the adsorbed globule regime; it hits the boundary between the adsorbed globule phase and the fence regime at $R^2/a^2N \sim 1/Z_*$. The desorbed-globule phase reappears for long polymers again below the full regime.

B. Repulsive Interactions between Blobs. For the adsorption on a plane and on a cylinder, we could neglect the repulsive interactions between adsorbed blobs; in those geometries, the blobs are not necessarily densely packed on the adsorbing surface, and the statistics of the chain of blobs can be studied independently of the blob statistics. In contrast, as the adsorption proceeds on a sphere, the blobs are packed denser and denser. When a certain number of monomers are adsorbed, the repulsive interactions between the adsorbed blobs gets stronger than the attraction to the sphere. We distinguish two different repulsive forces: (i) a repulsive three-body interaction, which becomes relevant at high monomer densities, and (ii) a repulsive electrostatic interaction between the induced dipoles. This last interaction can be estimated by calculating the field energy of a spherical capacitor. It is simply taken into account by introducing the effective charge of the sphere

$$Z_{\text{eff}} \equiv Z - g\sqrt{N_b f} \tag{42}$$

which is the bare charge of the sphere, Z, minus the charge of the inner capacitor sphere. The number of monomers per blob, $N_b = N/g$, is related to the effective charge by $N_b \sim \tilde{Z}_{\text{eff}}{}^{-2/3}R^2/a^2$ (see the discussion preceding eq 36). From this expression for N_b, eq 42, and the definition of the rescaled charge, eq 32, we obtain the number of blobs

$$g \sim (\tilde{Z} - \tilde{Z}_{\text{eff}})\tilde{Z}_{\text{eff}}{}^{1/3}\frac{Z_*{}^2}{\tilde{Z}^2} \tag{43}$$

The free energy of the adsorbed blob state is, in analogy to eq 36, given by

$$\frac{F}{k_BT} \sim g(1 - \tilde{Z}_{\text{eff}}{}^{2/3}) \sim \tilde{Z}_{\text{eff}}{}^{1/3}(1 - \tilde{Z}_{\text{eff}}{}^{2/3})(\tilde{Z} - \tilde{Z}_{\text{eff}})\frac{Z_*{}^2}{\tilde{Z}^2} \tag{44}$$

The value of $\tilde{Z}_{\text{eff}}$ is determined by minimization and given by

$$\tilde{Z}_{\text{eff}} = \tilde{Z}/2 + O(\tilde{Z}^{1/3}) \tag{45}$$

for the relevant case where $\tilde{Z}_{\text{eff}}$ is larger than unity. The number of blobs in the first complete layer, denoted by g_l, is, using eq 43, given by

$$g_l \sim \frac{Z_*{}^2}{\tilde{Z}^{2/3}} \tag{46}$$

The total number of monomers in the complete layer, denoted by N_l, is

$$N_l \equiv g_lN_b \sim \frac{Z_*{}^2R^2}{\tilde{Z}^{4/3}a^2} \sim \frac{Z^{2/3}R}{l_B{}^{1/3}a^{2/3}f^{2/3}} \tag{47}$$

where in the last expression we have pulled out the explicit dependence on the sphere radius R, which is linear. Conversely, the charged-monomer fraction f_l at which the first layer is full is given by

$$f_l \sim \frac{ZR^{3/2}}{al_B{}^{1/2}N^{3/2}} \tag{48}$$

This line is included in Figure 8 and divides the one-layer regime from the many-layers regime. To summarize this result: the charged sphere attracts and polarizes polyampholyte blobs until the resulting field inside the adsorbed blobs, which is the sum of the field of the sphere and the field due to the induced dipole moments of the polyampholyte, is roughly half of the bare field of the sphere. If the polymer is longer than N_l, the formation of a second layer of adsorbed polymer

is possible. The second layer obeys exactly the same laws as the first, with the only difference that the radius R entering the calculations is roughly twice as large.[20] This process of adsorbing more and more layers can continue, where we denote the total thickness of all layers by R_{tot}. The total number of monomers, N_{tot}, is given by the sum over the monomer numbers of all the adsorbed layers. Using eq 47 and assuming that we have n fully adsorbed layers, we obtain

$$N_{tot} = \sum_{i=1}^{n} N_l(i) \approx \frac{Z^{2/3} R}{l_B^{1/3} a^{2/3} f^{2/3}} \sum_{i=0}^{n-1} 2^i \tag{49}$$

With the approximation $\sum_{i=0}^{n-1} 2^i = 2^n - 1 \approx 2^n$ and the approximate identification $2^n R \approx R_{tot}$, we finally obtain for the relation between the total number of monomers and the total radius of the resulting multilayer structure the following equation:

$$N_{tot} \sim \frac{Z^{2/3} R_{tot}}{l_B^{1/3} a^{2/3} f^{2/3}} \tag{50}$$

For the adsorbed multilayer fence, as the layers pile up, the total radius can eventually become larger than the maximum radius of fence adsorption implied by eq 40. From eq 40 one obtains the maximal sphere radius for fence adsorption to be $R_{max} \sim Z^{2/3} a^{4/3} / l_B^{1/3} f^{2/3}$. The maximal number of monomers that can adsorb onto the sphere is, combining eq 40 and eq 50

$$N_{max} \sim \frac{Z^{4/3} a^{2/3}}{l_B^{2/3} f^{4/3}} \tag{51}$$

from which the charged-monomer fraction f_{max} at which the maximal number of monomers N are adsorbed within the multilayer structure is observed to be

$$f_{max} \sim \frac{Z a^{1/2}}{l_B^{1/2} N^{3/4}} \tag{52}$$

This line is included in Figure 8 and divides the full regime from the many-layers regime. For a longer PA chain, the adsorbed PA portion coexists with a globular fraction of the chain. That the non-adsorbed portion is globular (and not in a coillike state) is evident from the fact that the boundary between the full and many-layer regimes lies within the parameter range of the globular phase; see Figure 8. The radius of the adsorbed chain on the sphere at this threshold is, using eqs 50 and 51

$$R_{max} \sim \frac{N_{max} l_B^{1/3} a^{2/3} f^{2/3}}{Z^{2/3}} \sim a\sqrt{N_{max}} \tag{53}$$

and is independent of the radius of the sphere and roughly equals the Gaussian chain radius. This means that the average density in the adsorbed coil state at maximal filling equals the density in a Gaussian chain of the same number of monomers. This at first surprising result is easily understood since the total radius of the adsorbed chain is dominated by the outer layer, which is the thickest and which has Gaussian scaling. In contrast, the monomer density in the first full layer is

$$\rho_l \sim \frac{N_l}{R^3} \sim \frac{Z^{2/3}}{l_B^{1/3} a^{2/3} f^{2/3} R^2} \tag{54}$$

Comparing this density with the density in a globule, $\rho_g \sim N_D / R_D^3$, we find the ratio

$$\frac{\rho_l}{\rho_g} \sim \frac{Z^{2/3} a^{10/3}}{l_B^{4/3} f^{5/3} R^2} \tag{55}$$

Using the definitions for f_f^s and f_{ag}^s, the complete first layer is therefore denser than the globule for $f < (f_{ag}^s)^{4/5} (f_f^s)^{1/5}$; this boundary lies within the fence regime. For the case where the first complete layer is more compact than the globular state the three-body repulsion might be important and influence the phase boundary, but we did not pursue this point. The monomer density profile within the multiple-layer adsorbed state is given by

$$\rho(r) \sim \frac{N_l}{R r^2} \sim \frac{Z^{2/3}}{l_B^{1/3} a^{2/3} f^{2/3} r^2} \tag{56}$$

The density of the adsorbed state thus decreases towards the surface as the inverse square of the radial distance, but the total density equals the one of a Gaussian chain.

Our complete results for the adsorption of a polyampholyte chain on a sphere in the absence of salt are summarized in Figure 8. Within the adsorbed domain, we distinguish the regions of a single-coil (or pole), one incomplete layer, the region where one has one or more complete layers (note that this region is subdivided into regions distinguished by the number of adsorbed layers), and the region where the adsorbed layers coexist with an excess polyampholyte globule. The phase boundaries between these different phases scale as $f \sim N^{-2}$, N^{-3}, $N^{-3/2}$, and $N^{-3/4}$, respectively.

We wish to point out that the adsorbed polyampholyte, be it an incomplete layer or one or more layers, can be viewed as a *different globular state*, namely a densely packed state with a large net dipolar moment. The density in this state can in fact be higher or lower than the density in a normal globule, depending on the charged-monomer fraction f, compare eq 55. We believe that the present adsorption mechanism of a globular polyampholyte, namely the reorganization into a more ordered globular state of different structure, is a more general adsorption mechanism which could also apply to globular structures induced by short-range forces, as is the case in globular proteins. In that view, the present adsorption mechanisms could be a simple model for the interaction of proteins with binding sites and thus shed some light on problems such as recognition, acceptor/receptor reactions, and so on.

C. Effects of Added Salt. The overall effect of salt is to limit the maximal size of the adsorbed PA to the screening length. Inverting eq 50, we find the adsorbed multilayer structure to reach a thickness R_{tot} equal to the screening length κ^{-1} for

$$f_{max,s} \sim \frac{Z}{\kappa^{3/2} N^{3/2} l_B^{1/2} a} \sim \frac{f_l}{(\kappa R)^{3/2}} \tag{57}$$

On the basis of the phase diagram for the PA adsorption

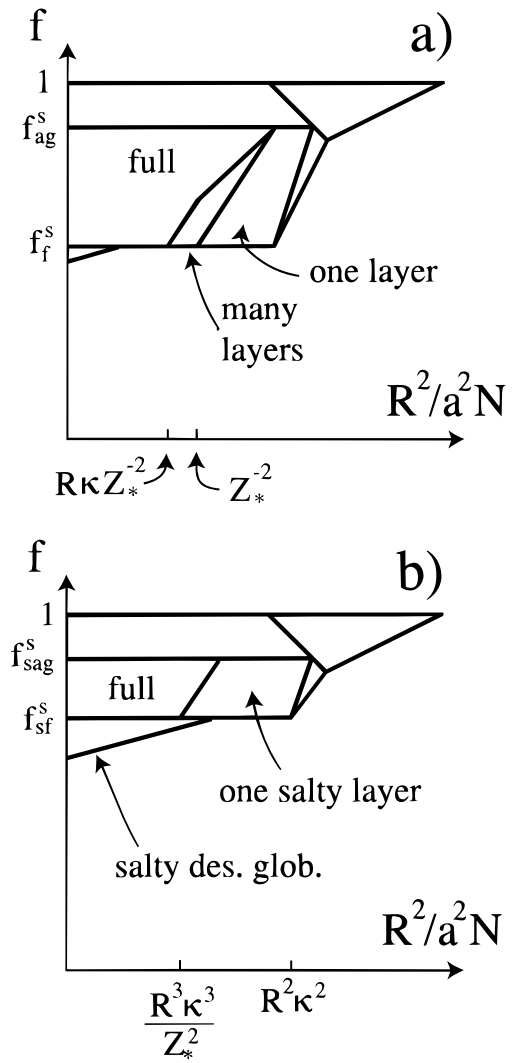

Figure 9. PA adsorption on a charged sphere in the presence of salt. (a) Screening length larger than the sphere radius R but smaller than the maximal adsorbate thickness, $RZ_*^2 > \kappa^{-1} > R$, where all multilayer structures which are thicker than the screening length are eliminated. (b) Screening length smaller than the sphere radius R but larger than the critical value beyond which no adsorption is possible at all, $R > \kappa^{-1} > R/Z_*^{2/3}$. Here the salt limits all adsorbed structures to a thickness of the screening length.

on spheres in the absence of salt, Figure 8, we briefly outline the resulting changes in the phase behavior.

(i) For $\kappa^{-1} > l_B Z^2$ there are no changes of the phase boundaries concerning adsorbed phases shown in Figure 8, because the fully adsorbed multilayer structure is always smaller than the screening length, as follows by comparison of eqs 52 and 57. The salty desorbed globule transforms into a (normal) desorbed globule for $f > f_{dg} \equiv a^2\kappa/l_B$ (compare with Figure 4c), which however does not influence the phase diagram in Figure 8 since the condition $f_{dg} < f^s_f$ is equivalent to $\kappa^{-1} > l_B Z^2$.

(ii) For $l_B Z^2 > \kappa^{-1} > R$, the screening length is larger than the thickness of the single-layer fence (and therefore does not change the single-layer fence structure), but the salt eliminates multilayer structures which have enough layers to reach a thickness larger than the screening length. This occurs for $f > f_{max,s}$ as given by eq 57. The resulting phase diagram is shown in Figure 9a.

(iii) For $R > \kappa^{-1} > R/Z_*^{2/3}$, there can only be one layer of adsorbed PA around the sphere, the thickness of which is reduced to the screening length. The transition from the pole regime to the fence regime occurs at $\tilde{Z} \sim \tilde{R}^3/\kappa R$, and this layer of thickness κ^{-1} is full for

$$f_{l,s} \sim \frac{f_l}{(\kappa R)^{1/2}} \tag{58}$$

as follows from a calculation similar to the one leading to eq 48. The resulting phase diagram is shown in Figure 9b. The salty fence regime exists for $f^s_{sf} < f < f^s_{sag}$ with $f^s_{sf} \equiv a^2R^4\kappa^4/Z^2l_B^2$ and $f^s_{sag} \equiv a^2Z/l_B^{1/2}\kappa^{1/2}R^2$. The transition between the partially filled layer and the full (single) layer, as determined by eq 58, hits the boundary between the fence and the desorbed regime, defined by $f = f^s_{sf}$, at $R^2/a^2N = R^3\kappa^3/Z_*^2$.

(iv) For $\kappa^{-1} < R/Z_*^{2/3}$ the screening length is the smallest length scale in the problem, and all adsorbed phases have disappeared. The resulting phase diagram is analogous to the one shown in Figure 4c, with a transition between a salty and a normal desorbed globular phase at $f \sim f_{dg} \equiv a^2\kappa/l_B$, and a meeting of all three phase separation lines at $N \sim N_s \equiv 1/a^2\kappa^2$.

All crossover scales occuring in Figures 8 and 9 are summarized in Table 3.

Table 3. Scaling Boundaries for the Adsorption on a Charged Sphere (Compare with Figures 8 and 9)

f^s_f	$a^2/l_B^2Z^2$	fence regime
f^s_{ag}	$Za^2/l_B^{1/2}R^{3/2}$	adsorbed globules
f^s_{sf}	$a^2\kappa^4R^4/l_B^2Z^2$	salty fence regime
f^s_{sag}	$Za^2/l_B^{1/2}R^2\kappa^{1/2}$	salty adsorbed globules

D. Charged Polyampholytes. Here we discuss the conditions under which a PA chain with a net charge of the same sign as a charged sphere can adsorb on the sphere. The case of a charged sphere deviates in one important point from the discussion for charged planes or cylinders: there it was found that salt is necessary for the adsorption to occur; otherwise the electrostatic repulsion is infinite. For the sphere, in contrast, the bare potential eq 29 goes to zero for large separations, and adsorption can occur even in the absence of salt. We therefore discuss the adsorption of similarly charged PA chains in the absence of added salt.

The repulsive energy due to the net charge is

$$\frac{W_{rS}}{k_BT} \sim \frac{\Delta fNZl_B}{R} \sim \frac{\Delta fRZl_B}{a^2}\frac{1}{\tilde{R}^2} \equiv \tilde{\Delta}f/\tilde{R}^2 \tag{59}$$

Comparing the repulsive energy with the free energy of the adsorbed globule phase, eqs 37 and 39, and the adsorbed coil and multiblob phase, eqs 35 and 36, one finds the sequence of modifications of the phase diagram for PA adsorption on a sphere in the absence of salt, shown in Figure 8:

(i) For $a^2Z^2/R^2 > \tilde{\Delta}f$ no change to the adsorbed phases occurs.

(ii) For $a^2Z^2/R^2 < \tilde{\Delta}f < 1$ the pole and fence regimes are not modified, but the adsorbed globule phase is eliminated for $f > a^4Z/R^3\Delta fl_B$.

(iii) For $1 < \tilde{\Delta}f < Z_*$ the pole regime is eliminated for $f < \tilde{\Delta}fR^2/NZ^2l_B^2$, which leads to a minimal charged-monomer fraction of $f \sim a^2\tilde{\Delta}f^{3/2}/Z^2l_B^2$ in order to obtain adsorption on the sphere.

(iv) For $Z_* < \tilde{\Delta}f < Z_*^2$ the adsorbed globule phase has disappeared, but the fence still exists in the range $a^2\tilde{\Delta}f^{3/2}/Z^2l_B^2 < f < f^s_{ag}$.

(v) For $Z_*^2 < \tilde{\Delta}f$ or $Z^2a^2/R^2 < \tilde{\Delta}f$ adsorption is no longer possible.

As a main result, charged spheres are quite effective in attracting PA of the same charge. The possibility of forming complexes between charged spheres and similarly charged PA chains opens up an intriguing gateway for forming *super-stable complexes*. This stands in vivid contrast to the complex formation between *dissimilarly* charged entities, where the resulting complex is normally less charged than the entities which formed the complex, and therefore the obtained colloidal suspension is less stable (for similar effects in the complexation behavior of charged polyampholytes, see ref 21). In the present case of complex formation between *similarly* charged entities, the resulting complex has a higher charge than each entity taken separately, and therefore the obtained colloidal suspension is even more stable than before the complex formation.

E. Multibody Effects. So far the calculation considered the adsorption of one polyampholyte on one charged sphere. Adsorption was considered to occur if the adsorption energy is larger than one k_BT. Clearly, this picture is incomplete. First, the energy necessary to form a stable complex is concentration dependent: for solutions where both the charged spherical objects and the polyampholyte chains are very dilute, the adsorption energy needs to be higher than k_BT. The results presented so far best describe the situation where one of the two components is rather concentrated, such that the chemical potential of the minority component in solution is not too high. Since most of the interesting effects obtain for globular polyampholytes, which are soluble only up to a very small concentration, the realistic scenario would be that of a moderately concentrated, charge-stabilized solution of spherical objects with a very small concentration of polyampholyte globules. Multibody effects become important in two different cases:

(i) In the case where there are precipitated polyampholyte globules in the system, this bottom phase acts as a reservoir, and multiple adsorption of polyampholyte globules onto one sphere becomes possible, if one is in the regime where the PA polymerization index is smaller than the maximal total number of adsorbed monomers, determined by eq 50. We note that this mechanism leads to large, spherical complexes, and not to gellike, extended objects. This is schematically shown in Figure 10a.

(ii) If there are very few polyampholyte globules in the system and if one is in the regime where the adsorbed polyampholyte coexists with a non-adsorbed globule part, the situation might arise that a single polyampholyte chain swallows up two or more charged spheres, as depicted in Figure 10b, part I. Here we denote the adsorbed dipolar PA portion by a gray region. It is easy to estimate the limit up to which the PA can adsorb spheres: from eq 44 we obtain the adsorption free energy for the first full layer to be $F/k_BT \sim Z_*^2 \sim Z^2l_B/R$. Any further adsorbed layer will further increase the adsorption energy, but each layer will contribute an adsorption energy smaller than the first layer and thus be an unimportant correction. We see that the adsorption energy is of the same order as the electrostatic repulsion between two spheres. We conclude that the PA will swallow charged spheres until the adsorbed layers (which have a thickness of the order of the sphere radius) touch each other. In this limit the whole PA is transformed into a coillike state, and behaves as a charged polymer, as depicted in Figure 10b, state III. In fact, the repulsion between neighboring blobs (each containing one charged sphere) is of the order of k_BT and is thus strong enough to stretch the polymer. However, the PA could transform into a necklace structure before it is close-packed with charged spheres, leading to the intermediate state II depicted in Figure 10b. To see whether state II occurs, we repeat the calculation leading to the necklace transition of a charged globule in section II.D: Balancing the electrostatic repulsion due to M spheres with charge Z each, swallowed by a globule of size R_g, $W_{el}/k_BT \sim l_BZ^2M^2/R_g$, with the surface energy $W_{surf}/k_BT \sim R_g^2/a^2N_D$, we obtain a necklace for a threshold sphere number $M_{nl} \sim (fN^{1/2}/Z$. The number of spheres corresponding to a close filling is $M_{cl} \sim R_g^3/R^3 \sim a^4N/l_BfR^3$. Comparing the two numbers, we see that $M_{nl} < M_{cl}$ is realized for $N > f^3R^6l_B^2/a^8Z^2$, i.e., for long PA chains, the PA transforms into a globular necklace (state II in Figure 10b) before the maximal number of adsorbed or swallowed spheres is reached.

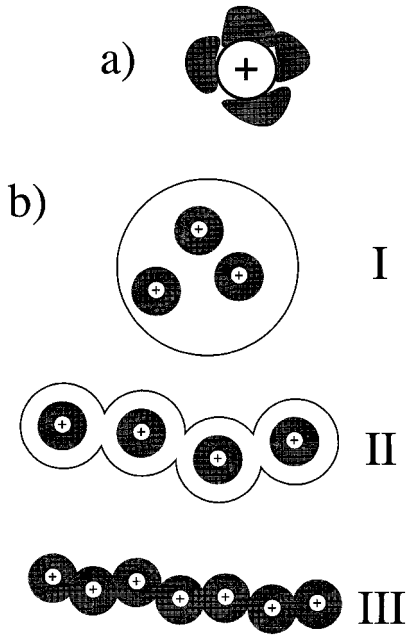

Figure 10. Schematic picture of multibody effects expected for the adsorption of PA chains on spherical charged spheres. (a) If there are more PA chains than spheres in the solution, multiple PA adsorption on a single sphere becomes possible, if one is not in the full regime, where a single PA chain basically swallows the sphere. (b) If there are more spheres than PA chains in the solution, a single PA chain can swallow many spheres if one is in the full regime (I). As the number of spheres increases, the PA globule can form a necklace structure, with one charged sphere per subglobule (II). As the number of adsorbed spheres reaches the limit where each sphere is surrounded by one adsorbate layer of thickness corresponding to the sphere radius, the polymer will form a stretched polyelectrolyte configuration (III). A direct transition from I to III is also possible.

This bridging mechanism can lead to a structure resembling a physical gel, because for a very long polyampholyte, the number of spheres connected by a single polyampholyte can be rather large. This is in agreement with experimental observations of an increased viscosity in gelatin/SDS[5−7] and PA/SDS[8] mixtures, which can be rationalized by an adsorption of chain sections on charged SDS micelles. Although not favored energetically, branching of the PA−sphere

complex is possible, even with a single PA molecule, leading to a network structure.

V. Discussion

We studied the adsorption behavior of single polyampholyte (PA) chains on charged objects of planar, cylindrical, and spherical geometry. We included the effects of added salt in the solution and of a net charge of the PA chains. Specific consideration was given to the influence of a coil−globular transition of the PA. In general, we find that short PA chains adsorb as a single coil, which is slightly stretched in order to maximize the attractive interaction between the spontaneous dipole moment of the PA coil and the charged object; this constitutes the pole regime. For longer chains, in the so-called fence regime, we observe the formation of a strongly adsorbed multiblob structure, which has a typical vertical size of the Gouy−Chapman length for the plane and of the cylinder or sphere radius. A slight modification of the vertical adsorbate size occurs for cylinders above the Manning condensation threshold, in which case the vertical size corresponds to the cylinder radius divided by the charge parameter, the latter being larger than unity. Cylinders and planes can be mapped onto each other by a simple rescaling of parameters, and they both show a weakly adsorbed multiblob regime, which is absent for spheres. Salt acts as to reduce the maximal allowed adsorbate size to the screening length and thus eliminates parts of the adsorbed phases obtained in the absence of salt. On the other hand, salt proves necessary in order to adsorb PA with a net charge similar to the object charge in the case of planes and cylinders. In general, the adsorption of similarly charged PA opens the way to producing colloidal dispersions of complexes for which the charge stabilization is even enhanced. A PA globule can either adsorb as an intact, whole globule or be dissolved into a strongly adsorbed coil.

For the adsorption onto spheres, we find that the repulsion of induced dipolar blobs is important for long PA chains and leads to a characteristic monomer density profile decaying as the inverse radial distance squared. For very long chains, the chain adsorbs only up to a certain chain length, and the remaining part of the chain is unperturbed. This constitutes a simple mechanism for the gelation of PA/charged sphere mixtures, since the PA-section unused for the adsorption on one sphere can span the distance to a second sphere and so on, leading to a quite extended, multisphere object. Similar conclusions have been drawn from experiments on the complexation behavior of gelatin (a biopolyampholyte) or synthetic PA with SDS (a charged surfactant forming spherical, strongly charged, micelles).

It would be interesting to extend the current study to the case of PA solutions, in which case interchain interactions would have to be taken into account. To a first approximation, the effect of a finite concentration of PA or charged objects enters our calculation via the in this case finite screening length. In a more refined calculation, one expects characteristic adsorbed density profiles, much as obtained for the single-chain adsorption on a sphere.

Acknowledgment. We acknowledge useful discussions with F. Candau and I. M. Harrison.

Appendix A: Poisson−Boltzmann Equation for one Isolated Cylinder

The exact solution of the Poisson-Boltzmann equation for a periodic array of infinitely long cylinders in the presence of counterions but without salt has been published long time ago.[22] Some approximate solutions have been given for a single cylinder with counterions and salt.[23] Here we present the exact analysis for the limiting case of one single, isolated cylinder without salt, which illustrates the occurrence of Manning condensation in a very clear fashion.

Combining Laplace's equation

$$\Delta\psi(\mathbf{r}) = -\frac{e}{\epsilon}n(\mathbf{r}) \tag{A1}$$

where $n(\mathbf{r})$ denotes the counterion density and $\psi(\mathbf{r})$ the electric potential, with the Boltzmann equation

$$n(\mathbf{r}) = n_0 \exp\left\{-\frac{e\psi(\mathbf{r})}{k_B T}\right\} \tag{A2}$$

one obtains at the Poisson−Boltzmann (PB) equation, which for cylindrical symmetry reads

$$\left[\frac{d^2}{dr^2} + \frac{1}{r}\frac{d}{dr}\right]\psi(r) = -\frac{en_0}{\epsilon}\exp\left\{-\frac{e\psi(r)}{k_B T}\right\} \tag{A3}$$

In the following we consider a charged cylinder with a radius R. The constant n_0 is defined by $n(R) = n_0$ and thus denotes the counterion density at the cylinder surface, from which follows $\psi(R) = 0$. Clearly, the ion density vanishes at infinity, from which follows that $\psi(\infty) = \infty$. The electric field satisfies the following boundary condition at the cylinder surface

$$\left.\frac{d\psi(r)}{dr}\right|_{r=R} = \frac{\tau}{2\pi R\epsilon} \equiv \frac{2k_B T\tilde{\tau}}{eR} \tag{A4}$$

The parameter τ denotes the charge density per unit length on the cylinder, the parameter $\tilde{\tau} = l_B\tau/e$ is the reduced charge parameter of the cylinder. Using the definitions

$$u \equiv \ln(r/R) \tag{A5}$$

and

$$v \equiv -\frac{e\psi}{k_B T} + 2\ln(r/R) \tag{A6}$$

the PB equation can be rewritten as

$$\frac{d^2 v(u)}{du^2} = \kappa^2 e^{v(u)} \tag{A7}$$

with the definition

$$\kappa^2 \equiv \frac{n_0 e^2 R^2}{\epsilon k_B T} \tag{A8}$$

The boundary condition eq A4 in the new coordinates reads

$$\frac{dv}{du} = 2(1 - \tilde{\tau}) \tag{A9}$$

The first integral of the PB equation eq A7 can be performed, and the equation determining $v(u)$ is given by

$$\left(\frac{\mathrm{d}v(u)}{\mathrm{d}u}\right)^2 = 2\kappa^2 e^{v(u)} + 4C \tag{A10}$$

with the definition

$$C \equiv (1-\tilde{\tau})^2 - \kappa^2/2 \tag{A11}$$

The solution is fully determined by the integral expression

$$I(v) \equiv \int \frac{\mathrm{d}v}{\sqrt{2\kappa^2 e^v + 4C}} \tag{A12}$$

which depends on the sign of C and is given by

$$I(v) = \begin{cases} -C^{-1/2}\,\mathrm{arctanh}(1+\kappa^2 e^v/2C)^{-1/2} & \text{for } C > 0 \\ -\sqrt{2}e^{-v/2}/\kappa & \text{for } C = 0 \\ -(-C)^{-1/2}\arctan(-1-\kappa^2 e^v/2C)^{-1/2} & \text{for } C < 0 \end{cases} \tag{A13}$$

For the case of one isolated cylinder and for $\tilde{\tau} > 1$, the solution is obtained with $C = 0$ and reads

$$v(u) = -2\ln(1+\kappa u/\sqrt{2}) \tag{A14}$$

From the boundary condition eq A9 one obtains that $\kappa = 2^{1/2}(\tilde{\tau}-1)$, which is valid only for $\tilde{\tau} - 1$. For smaller values of $\tilde{\tau}$ the constant κ equals zero (no counterions are bound to the cylinder) and thus

$$v(u) = 2u(1-\tilde{\tau}) \tag{A15}$$

For the potential distribution we thus obtain the final result

$$\frac{e\psi(r)}{k_B T} = \begin{cases} 2\left\{\ln\left[\frac{r}{R}\right] + \ln\left[1 + (\tilde{\tau} - 1)\ln\left(\frac{r}{R}\right)\right]\right\} & \text{for } \tilde{\tau} \geq 1 \\ 2\tilde{\tau}\ln\left[\frac{r}{R}\right] & \text{for } \tilde{\tau} \leq 1 \end{cases} \tag{A16}$$

For small charge parameters $\tilde{\tau} \leq 1$ no counterions are bound to the cylinder and the potential distribution corresponds to the bare logarithmic potential. For larger charge parameters, a finite fraction of counterions is bound to the charged cylinder; this phenomenon is called Manning condensation.[18] The total number of ions which are bound to the cylinder per unit length, N_B, is

$$N_B \equiv 2\pi\int_R^\infty \mathrm{d}r\, rn(r) \tag{A17}$$

which is, using the definitions and results from this section, given by

$$N_B = \frac{2\pi n_0 R^2}{\tilde{\tau} - 1} \tag{A18}$$

The *capture ratio*, i.e., the fraction of ions which are bound to the cylinder, is

$$\frac{N_B}{\tau/e} = \frac{\tilde{\tau} - 1}{\tilde{\tau}} \tag{A19}$$

As expected, this ratio approaches unity for very large charge parameter (i.e., essentially all counterions are bound to the cylinder) and goes to zero as the charge parameter decreases towards $\tilde{\tau} = 1$; i.e., the fraction of bound counterions goes to zero. This is the signature of the Manning condensation threshold. To obtain a feeling for the characteristics of the adsorbed counterion cloud, we calculate the distance within which a certain fraction ϕ of the bound counterions (N_B) is localized. This means, we solve the equation

$$2\pi\int_R^D \mathrm{d}r\, rn(r) = N_B\phi \tag{A20}$$

leading to

$$D = \mathrm{R}\exp\left[\frac{\phi}{(1-\phi)(\tilde{\tau}-1)}\right] \tag{A21}$$

This demonstrates two important facts about Manning condensation: (i) the layer of condensed counterions is rather diffuse if $\tilde{\tau}$ is not much larger than unity (in fact, the width for any fraction ϕ larger than zero goes to infinity as one approaches the Manning threshold), and (ii) the counterion concentration is continuous close to the cylinder surface. Within the simple model studied here, the fraction of counterions bound on the surface is zero.

The potential distribution above the Manning threshold shows distinctive different behaviors close to the cylinder and far away. For separations $r \gg R$, the potential behaves like for a cylinder with a charge parameter at the Manning threshold plus logarithmic corrections, i.e.

$$\frac{e\psi(r)}{k_B T} \simeq 2\left\{\ln\left[\frac{r}{R}\right] + \ln\left[\ln\left(\frac{r}{R}\right)\right]\right\} \tag{A22}$$

Closer to the cylinder surface, i.e., using the definition $r = R + x$ and for $x < R$, the potential asymptotically merges into the solution expected in the vicinity of a planar surface

$$\psi(r) \simeq \frac{2k_B T}{e}\ln[1 + \tilde{\tau}x/R] \tag{A23}$$

The Gouy−Chapman length that characterizes the decay of the counterion density close to the surface is $\lambda_C = R/\tilde{\tau}$ and is given by the standard formula eq 2 if one uses for the surface charge density at the cylinder surface the expression $\sigma_C = \tau/2\pi R$. It is smaller than the radius of the cylinder.

Appendix B: Residual Dipole Moment of a Polyampholyte Globule

In this section we are interested in the dipole moment, or, equivalently, in the amount of uncompensated charges within a collapsed polyampholyte chain. To see that this case is much more complicated than an *uncollapsed* polyampholyte coil, let us start with some simple considerations. As argued before, for a PA chain of N monomers, one divides the coil arbitrarily into halves, which on average have typical (dimensionless) net charges of magnitude $\tilde{Q} \sim (fN)^{1/2}$. The electrostatic energy (taking as the reference state the electricfield-free case) associated with this dipole is $W/k_B T \sim \tilde{Q}^2 l_B/R$.

This energy results from the energy needed to create the two opposing (roughly spherical) charge distributions of different sign, minus the energy gained by putting these charge clouds close to each other. The resulting energy is positive, which follows from the fact that the electric field is not identically zero (and from remembering that the total electric energy is proportional to the electric field squared). For a Gaussian coil one has a radius of $R \sim aN^{1/2}$, so that the dipolar energy reads

$$\frac{W}{k_B T} \sim \sqrt{N}\,\frac{f l_B}{a} \sim \sqrt{\frac{N}{N_D}} \tag{B1}$$

The chain length at which this dipolar energy becomes unity coincides with the chain length of a Debye blob, $N_D = a^2/l_B^2 f^2$. This is expected, because it is the electrostatic attraction between unlike charges which is responsible for the chain collapse in the first place. For a chain length larger than N_D, the electrostatic energy is larger than the thermal energy. Therefore, the residual dipole moment in a polyampholyte globule should be significantly smaller than a argument similar to the one given above for the polyampholyte coil would predict. In other words: the attraction between unlike charges is the driving force for the polyampholyte collapse. It is therefore expected that the amount of uncompensated charges is smaller than predicted by a noninteracting model.

To make some progress on this complicated question, we suggest the following model: the collapsed state can be envisioned as a superposition of g Gaussian coils, each consisting of N/g monomers and of the spatial size of the globule. This requirement fixes the number of coils, g, which is determined by equating the globule radius with the Gaussian radius, $R_g \sim aN_D^{1/6}N^{1/3} \sim a(N/g)^{1/2}$. Each Gaussian blob should exhibit unperturbed chain statistics, and in particular have $\tilde{Q}_b \sim (fN/g)^{1/2}$ separated charges for an arbitrary cut into halves. This picture of unperturbed, Gaussian statistics for a subchain size smaller than the globule radius agrees with the original Lifshitz description of the coil−globular phase transition.[24] Each Gaussian chain has a permanent dipole moment $\mathbf{p}_m = e\tilde{Q}_b R_g \mathbf{s}_m$ where $\mathbf{s}_m$ is a unit vector which points in the direction of the permanent dipole. The total dipole moment $\mathbf{P}$ of the globule can be calculated by summing over the individual dipoles, $\mathbf{P} = \sum_m \mathbf{p}_m$. The self energy associated with the total dipole moment is

$$\frac{U}{k_B T} = \frac{P^2 l_B}{e^2 R_g^3} = \eta[\sum \mathbf{s}_m]^2 \tag{B2}$$

where the coupling constant is

$$\eta \equiv \tilde{Q}_b^2 \frac{l_B}{R_g} = f\frac{l_B}{a}\sqrt{\frac{N}{g}} \tag{B3}$$

In writing down the interaction energy we assume that the dipoles consist of oppositely charged diffuse clouds, each cloud of the radius of about the distance between the clouds. The partition function of a system of g interacting dipolar coils is therefore given by

$$Z = \prod_{n=1}^{g}[\int \mathrm{d}\mathbf{s}_n\, \delta(1 - |\mathbf{s}_n|)] \exp\{-\eta[\sum_m \mathbf{s}_m]^2\} \tag{B4}$$

This expression neglects the electrostatic energy associated with the coupling between higher multipoles. These energies are important for the calculation of the free energy itself; in this section, however, we are only interested in the *effective dipole moment* of a PA globule and use the fact that higher multipole moments do not couple to the dipole moment. We therefore believe that, although the free energy following from this partition function is incorrect (taken as it is, the partition function does not reproduce the parameter dependence of the coil-globule transition in agreement with ref 3), the resulting dipole moment is correct, if one uses for the blob number g the correct values as predicted by Higgs and Joanny. This conjecture is substantiated by the fact that the resulting dipole moment of a globule, presented in eq B11, agrees with the naive guess $\tilde{Q} \sim fN^{1/2}$ at $N = N_D$ and therefore joins continuously at the coil−globule transition and that the electrostatic energy associated with the uncompensated charges stays constant at a value of $(^3/_2)\, k_B T$ (compare with eq B10) in the globular phase, which one would obtain from a simple scaling argument using thermal fluctuations.

After a Hubbard−Stratonovich transformation, the partition function reads

$$Z = \frac{1}{(4\pi\eta)^{3/2}}\int \mathrm{d}\mathbf{w} \prod_{n=1}^{g}[\int \mathrm{d}\mathbf{s}_n\, \delta(1 - |\mathbf{s}_n|)] \exp\left\{-\frac{\mathbf{w}^2}{4\eta} - i\mathbf{w}\sum_m \mathbf{s}_m\right\} \tag{B5}$$

The integral over the Heisenberg spin variables can be performed, and the resulting expression is

$$Z = (4\pi)^g \left(\frac{1}{4\pi\eta}\right)^{3/2} \int \mathrm{d}\mathbf{w} \exp\left\{-\frac{w^2}{4\eta}\right\}\left(\frac{\sin w}{w}\right)^g \tag{B6}$$

In the interesting limit of large g the integrand consists of sharp, delta-like peaks, for which a saddle-point approximation can be used. It turns out that the saddle point located at $w = 0$ is dominant, for which we use the relation

$$\left(\frac{\sin w}{w}\right)^g \simeq \exp(-gw^2/6) \tag{B7}$$

The final result is

$$Z \simeq (4\pi)^g (1 + 2\eta g/3)^{-3/2} \tag{B8}$$

We can now calculate the expectation value of the reduced, squared dipole moment

$$\langle[\sum_m \mathbf{s}_m]^2\rangle = -\frac{\partial(\ln Z)}{\partial\eta} = \frac{3}{2}\eta^{-1} \tag{B9}$$

From the relation $\mathbf{P} = e\tilde{Q}_b R_g \sum_m \mathbf{s}_m$ and the definition of η, we obtain the average squared dipole moment of the globule, $\langle \mathbf{P}^2\rangle = 3e^2 R_g{}^3/(2l_B)$, and the polarizability of the globule, $\alpha = \langle \mathbf{P}^2\rangle/3k_B T = e^2 R_g{}^3/(2k_B T l_B)$. The internal energy is

$$\left\langle \frac{U}{k_B T}\right\rangle = \eta\langle[\sum_m \mathbf{s}_m]^2\rangle = \frac{3}{2} \tag{B10}$$

We obtain the interesting result that the internal energy

remains constant at a value of $^3/_2$, independent of the number of overlapping coils g (in the limit of large g) and on the interaction parameter. The strong interaction between all fluctuating dipoles brings down the effective number of degrees of freedom to three, the number of spatial coordinates. From the expectation value of the dipole moment $\langle P^2 \rangle$, it is easy to calculate the total number of separated charges in a globule, $\tilde{Q}_g$. Using that the globule radius is given by $R_g \sim a(aN/fl_B)^{1/3}$ we obtain for the number of separated charges in the globule

$$\tilde{Q}_g = \frac{P}{eR_g} = \left(\frac{N}{f}\right)^{1/6}\left(\frac{a}{l_B}\right)^{2/3} = N^{1/6}N_D{}^{1/3}f^{1/2} \quad \text{(B11)}$$

which is smaller than the naive guess $\tilde{Q} \sim (fN)^{1/2}$ and only agrees with this guess at the collapse transition, for $N = N_D \sim (a/l_B f)^2$.

We can now estimate the effect of an external field E on the globule. For a free energy associated with the orientation of the permanent total dipole moment in the external field smaller than k_BT (in which case the orientation is rather weak) it can be obtained from the polarizability

$$\frac{F}{k_BT} = -\frac{1}{2}\frac{\alpha E^2}{k_BT} \sim -\frac{E^2e^2R_g{}^3}{(k_BT)^2l_B} \sim -\frac{NE^2e^2a^4}{(k_BT)^2fl_B{}^2} \quad \text{(B12)}$$

For larger fields the PA globule is oriented completely, in which case the free energy is

$$\frac{F}{k_BT} = -\frac{EP}{k_BT} \sim -\frac{Ee\tilde{Q}_gR_g}{k_BT} \sim -\frac{Eea^2}{k_BTl_B}\sqrt{\frac{N}{f}} \quad \text{(B13)}$$

The value of the electric field where these free energies are both of order unity is

$$\frac{Ee}{k_BT} = \frac{l_Bf^{1/2}}{a^2N^{1/2}} \quad \text{(B14)}$$

which gives the threshold above which the electric field is strong enough to perturb or deform the globule. At very high electric field strengths the globule is dissolved into a strongly stretched polyampholyte coil. This transition field strength can be estimated from comparing the free energy of a polyampholyte globule

$$\frac{F}{k_BT} \sim -N\left(\frac{fl_B}{a}\right)^2 \quad \text{(B15)}$$

and the free energy of a stretched PA coil under the action of a strong external field

$$\frac{F}{k_BT} \sim -fN^2a^2\left(\frac{eE}{k_BT}\right)^2 \quad \text{(B16)}$$

The transition field strength is given by the value at which the two free energies are equal and agrees with the estimate eq B14 for the threshold at which the globule is perturbed. Our conclusions for the effect of an external electric field on a collapsed PA globule is that the response of a globule to an external electric field is rather weak and consists of a partial orientation of the residual dipole moment parallel to the electric field. The threshold at which the electric field is strong enough to fully orient the globule and to deform the globule coincides with the dissolution transition into a stretched coil. This is the result of a minimal model, which however should capture the essential physics. A more microscopic approach might reveal a smooth change at the crossover regime between the weak response case (for small fields where the interaction energy is much smaller than unity) and the strong response case (where the electric field is strong enough to completely dissolve the globule). For the interaction of a polyampholyte globule with a charged object, the situation is actually more complicated, because here the electric field is not homogeneous and typically acts only over a short distance. Here one has to compare the electrostatic energy of the oriented globule (which can be calculated using eq B11) with the energy of the dissolved coil in the nonhomogeneous electric field. As a result, the adsorption of the globule as a whole can in fact be favored over the dissolution into a coil for this case.

References and Notes

(1) Barrat, J.-L.; Joanny, J.-F. *Adv. Chem. Phys.* **1996**, *94*, 1.

(2) Edwards, S. F.; King, P. R.; P. Pincus, *Ferroelectrics* **1980**, *30*, 3.

(3) Higgs, P. G.; Joanny, J.-F. *J. Chem. Phys.* **1988**, *89*, 5273.

(4) Candau, F.; Joanny, J.-F. In *Polymeric Materials Encyclopedia*; Salamone, J. C., Ed.; CRC Press, Boca Raton, FL, 1996.

(5) Greener, J.; Contestable, B. A.; Bale, M. D. *Macromolecules* **1987**, *20*, 2490.

(6) Cosgrove, T.; White, S. J.; Zarbakhsh, A.; Heenan, R. K.; Howe, A. M. *J. Chem. Soc., Faraday Trans.* **1996**, *92*, 595.

(7) Griffiths, P. C.; Stilbs, P.; Howe, A. M.; Whitesides, T. H. *Langmuir* **1996**, *22*, 5302.

(8) Harrison, I. M.; Candau, F.; Zana, R. To be published.

(9) Neyret, S.; Ouali, L.; Candau, F.; Pefferkorn, E. *J. Colloid Intface Sci.* **1995**, *176*, 86.

(10) Joanny, J.-F. *J. Phys. II Fr.* **1994**, *4*, 1281.

(11) Dobrynin, A. V.; Rubinstein, M.; Joanny, J.-F. *Macromolecules* **1997**, *30*, 4332.

(12) Schiessel, H.; Blumen, A. *J. Chem. Phys.* **1996**, *104*, 6036; *Macromol. Theory Simul.* **1997**, *6*, 103.

(13) Israelachvili, J. N. *Intermolecular and Surface Forces*; Cornell Univ. Press: Ithaca, NY, 1985.

(14) Kantor, Y.; Kardar, M. *Europhys. Lett.* **1991**, *14*, 421; **1994**, *27*, 643.

(15) Gutin, A.; Shakhnovich, E. *Phys. Rev. E* **1994**, *50*, R3322.

(16) Dobrynin, A. V.; Rubinstein, M. *J. Phys. II Fr.* **1995**, *5*, 677.

(17) Borisov, O. V.; Zhulina, E. B.; Birshtein, T. M. *J. Phys. II Fr.* **1994**, *4*, 913.

(18) Manning, G. S. *J. Chem. Phys.* **1969**, *51*, 954.

(19) Alexander, S.; Chaikin, P. M.; Grant, P.; Morales, G. J.; Pincus, P.; Hone, D. *J. Chem. Phys.* **1984**, *80*, 5776.

(20) This procedure is in fact not totally correct: In principle, one should treat all layers simultaneously and calculate the resulting monomer distribution by equating the monomer chemical potentials in each layer. But on a more fundamental level also the partitioning of the adsorbed PA coils into separate and not interpenetrating layers is a questionable concept, which we chose for mathematical simplicity. Building the total adsorbate layer by layer (without equating chemical potentials) is an error of the same order as the model itself. In fact, the transition to the full region is exact (within the layer model), because here we explicitly equate the chemical potentials with the chemical potential in a nonadsorbed globule.

(21) Everaers, R.; Johner, A.; Joanny, J.-F. *Europhys. Lett.* **1997**, *37*, 275.

(22) Fuoss, R. M.; Katachalsky, A.; Lifson, S. *Proc. Natl. Acad. Sci. U.S.A.* **1951**, *37*, 579.

(23) Philip, J. R.; Wooding, R. A. *J. Chem. Phys.* **1970**, *52*, 953.

(24) Lifshitz, I. M. *Zh. Eksp. Teor. Fiz. Nauk* **1968**, *55*, 2408; *Sov. Phys. JETP* **1969**, *28*, 1280.

MA980115B